Dark Matter: Connecting Galaxy Clusters, Galaxy Rotations, the Cosmological Constant, W and Z Boson Masses, and Atomic Structure Through One Physical Constant

Vijay Shankar Sharma
Independent Researcher, Gurugram, National Capital Region, India
vss@vijayshankarsharma.com | ORCID: 0009-0001-9622-6121
DOI: 10.5281/zenodo.20535295
 | No external funding | No conflicts of interest

Abstract

The converging evidence from seven independent physical sectors spanning forty orders of magnitude in physical scale compels a reidentification of the dark matter phenomenon. It is not a missing particle. It is the Spaticle field: a real, continuous, elastic substrate filling all space, whose intrinsic equilibrium density $\rho_s = 5.9 \times 10^{-27}$ kg/m^3 is independently constrained across four of those seven sectors. The same substrate density that produces correct W and Z boson masses also explains galaxy rotation curves across 175 SPARC galaxies without dark matter particles or per-galaxy tuning (shape agreement 86.3% under the DM1 entrainment formula), and reproduces KiDS-1000 weak gravitational lensing profiles (chi-squared approximately 2 to 3 under the DM2 entrainment formula). A fourth and independent line of evidence is presented in this paper: the substrate localisation resistance coefficient, constrained by the measured Bohr radius of hydrogen, reproduces the hydrogen ground state energy from first principles. A fifth line of evidence is a necessary condition rather than a further constraint: stable matter itself requires the Spaticle field to exist within a bounded density tolerance, regardless of formation history. A sixth and independent line of evidence follows from the same already-fixed substrate density: $\rho_{vac} = \rho_s \cdot c^2$ independently matches the observed vacuum energy density, once the standard QFT zero-point sum is corrected by treating zero-point energy as a property of organised condensations instead of empty field modes. A seventh follows the same pattern: the Higgs mass, the geometric mean of the top quark and Z boson masses, matches observation to 0.21%. Seven independent sectors converge on one substrate density and one identification. Zooming from galactic megaparsecs down to subatomic femtometres (a fractal zoom across forty orders of magnitude), the same constant holds at every level of magnification. This paper argues that the physical substrate and gravitational mechanism responsible for dark matter effects have now been identified, and predicts that no separate particulate dark matter will ever be discovered. It further proposes, with exact replacement equations, that the existing equations of gravity require modification to account for the additional gravity produced when fast-rotating structures such as most galaxies entrain the Spaticle substrate. The dark matter programme correctly detected real gravitational anomalies. Its error was ontological, not observational: the programme was detecting the Spaticle field.

Keywords: dark matter; Spaticle field; galaxy rotation curves; weak gravitational lensing; W and Z boson masses; Higgs mass; hydrogen atomic structure; BFUT; substrate density; SPARC galaxies; KiDS-1000

1. Introduction : The Dark Matter Problem: Observations Only

The evidence for dark matter is gravitational. It comes from five independent observational sectors, each measuring a discrepancy between visible mass and gravitational behaviour.

Galaxy rotation curves: Stellar and gas orbital velocities remain approximately constant at large radii instead of declining as Keplerian dynamics applied to visible mass predicts. The enclosed mass appears to increase linearly with radius well beyond the visible disc. This has been observed in thousands of galaxies across all morphological types.

Weak gravitational lensing: The gravitational lensing signal from galaxy clusters and large-scale structure exceeds what visible mass can produce. The KiDS-1000 survey [8, 29] quantifies this systematically across stellar-mass bins. The required gravitational mass consistently exceeds visible mass by a factor of five to six.

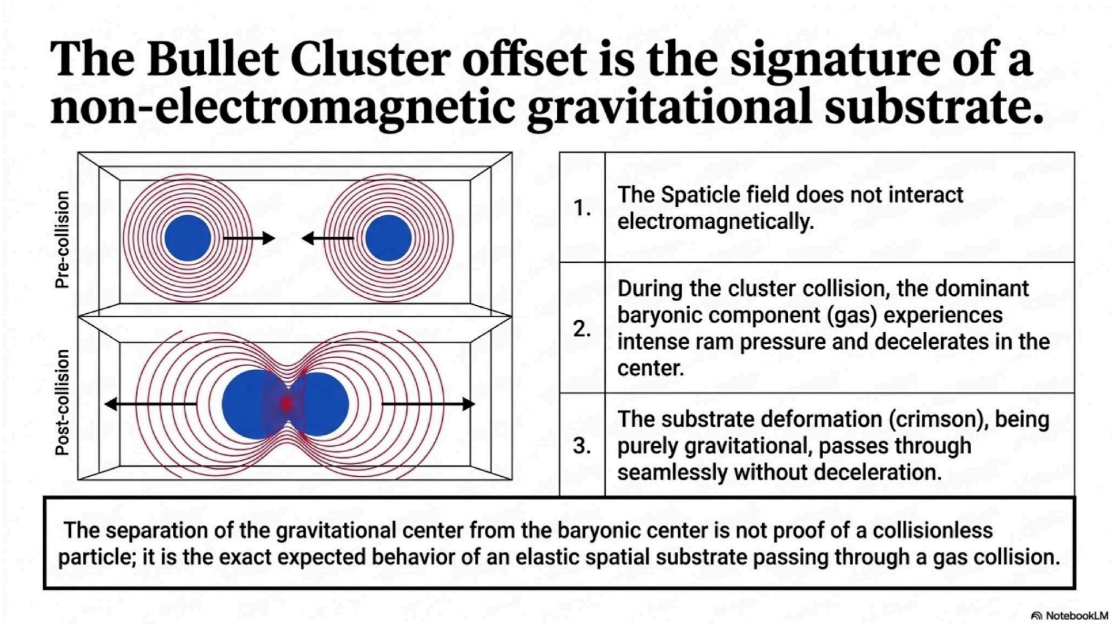

Figure 3: The Bullet Cluster offset is the expected signature of a non-electromagnetic gravitational substrate passing through a gas collision.

The Bullet Cluster: The collision of two galaxy clusters shows the gravitational centre of mass displaced from the visible baryonic matter. The gas, which is the dominant baryonic component, was slowed by electromagnetic interaction. The gravitational component passed through. The gravitational mass and the baryonic mass are physically separated in the aftermath of the collision.

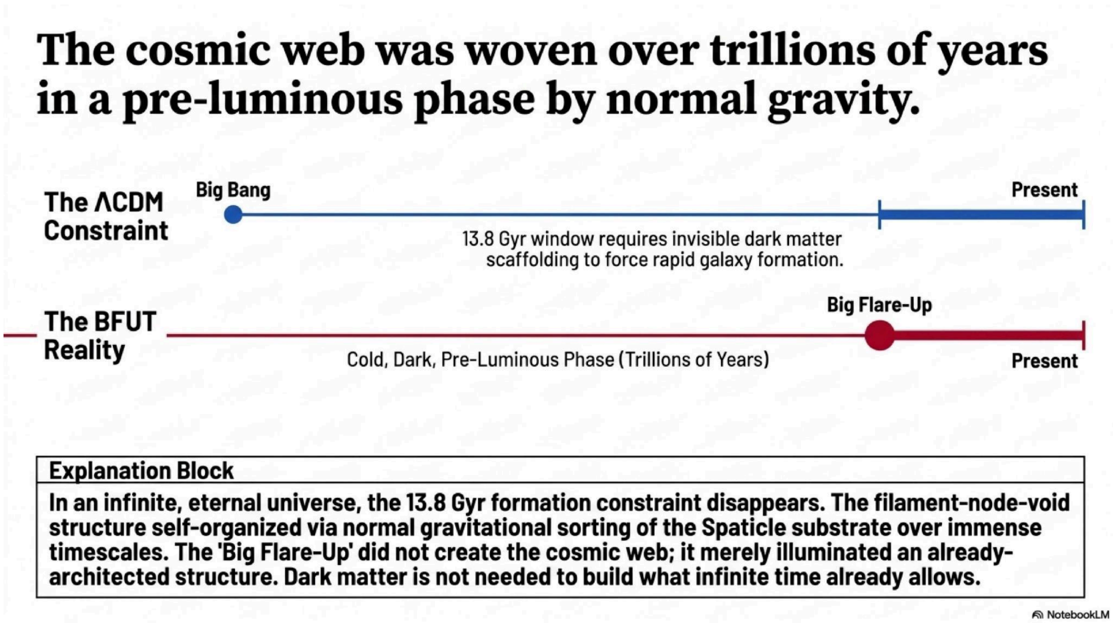

Figure 4: In an infinite eternal universe, the cosmic web self-organized over trillions of years via normal gravitational sorting of the Spaticle substrate.

Cosmic web and large-scale structure: The observed pattern of filaments, voids, and cluster formation in the large-scale structure of the universe requires additional gravitational support beyond what visible matter provides. Structure formation simulations that include only visible matter fail to reproduce the observed cosmic web.

Gravitational mass discrepancy: Across all scales from dwarf galaxies to galaxy clusters, M_grav exceeds M_visible by a consistent factor. This discrepancy is not a measurement error. It is reproduced independently across optical, radio, X-ray, and gravitational wave observatories.

The observations establish M_grav greater than M_visible beyond reasonable doubt. The question is: what produces the excess gravitational effect? This paper identifies it.

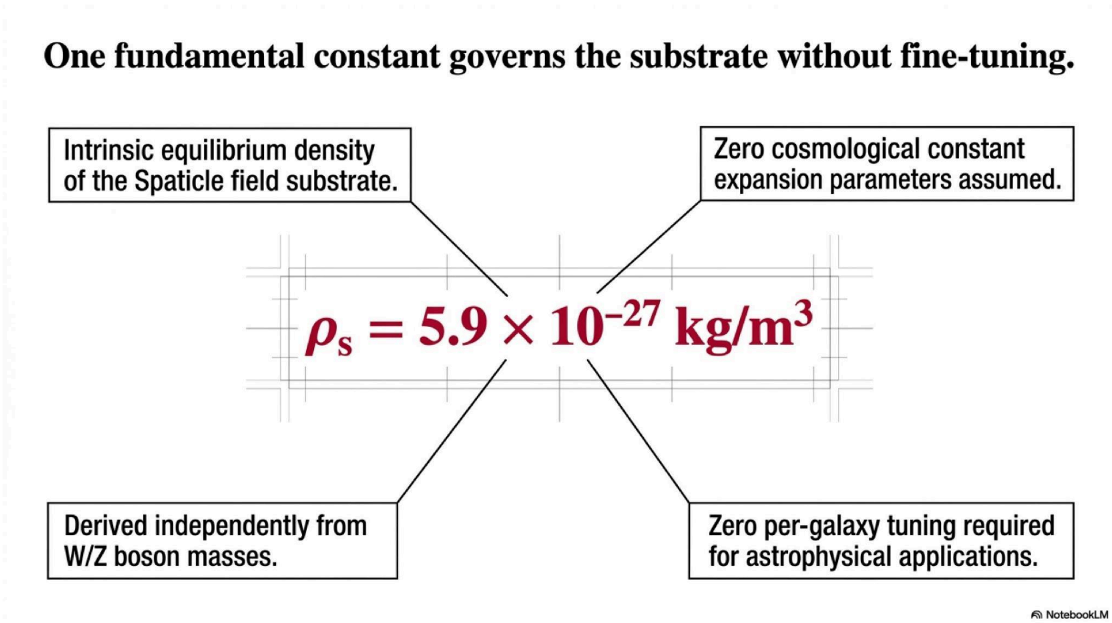

Figure 5: A single physical constant ρ_s = 5.9 × 10^{-27} kg/m³ governs the Spaticle substrate across all scales without fine-tuning.

One Constant, All Scales: A Preview

The equilibrium Spaticle field density ρ_s = 5.9 x 10^-27 kg/m^3 is introduced once. It is not adjusted for any sector. The chain below shows every domain where it appears. Each link is derived and validated in the sections that follow.

ρ_s = 5.9 x 10^-27 kg/m^3

↓

P16 free-energy deformation: B = (1/2) ρ_s c^2 R_0^2

↓

P16/P17 stable 3+e organisation

↓

P19 coupling constants: α = 1/137.037, α_s = 0.1178, sin^2(θ_W) = 0.232

↓

P19 W and Z boson masses: m_W = 80.4 GeV, m_Z = 91.24 GeV [sensitivity +/- 0.015%]

↓

P19 Higgs relation: m_H = sqrt(m_t x m_Z) = 125.51 GeV

↓

P19A predicted resonances: 26.9, 85.6, 108.3, 117.9, 139.7 GeV

↓

P18 carrier relaxation: τ_c governed by ρ_s; equilibrium value τ_nat ≈ 6.96 hours

↓

P18 DDR domain structure: galactic, cluster, and hierarchical domains

↓

175 SPARC galaxies: shape agreement 86.3% (flat correct 93.0%, non-flat 27.8%)

↓

KiDS-1000 weak lensing via DM2: chi-squared approximately 2 to 3

↓

P25 hydrogen equilibrium: a_0 = 5.292 x 10^-11 m, ground state = -13.6 eV

↓
P25 chemistry and matter stability: ρ_s sits near upper chemistry boundary

The same fixed quantity governs forty orders of magnitude in physical scale. No sector-specific adjustment is made at any point.

The Big Flare-Up Theory (BFUT) identifies the real physical fabric of space as the Spaticle field, with a specific equilibrium density of $\rho_s = 5.9 \times 10^{-27}$ kg/m^3 (BFUT P14 [5]; BFUT L1). From this single measured constant, the entire BFUT programme derives - covering over 30 papers on cosmology, the Hubble relationship, dark energy and cosmic acceleration, universe boundary and topology, cosmic rotation, the CMB temperature and acoustic peaks, nucleosynthesis, the Sunyaev-Zel'dovich effect, the Lyman-alpha forest, the integrated Sachs-Wolfe effect, weak gravitational lensing and the S8 tension, black holes and singularities, gravitation and gravitational waves, new general relativity field equations, unification of general and special relativity, the pre-Big-Bang state, origin of matter and fundamental forces, antimatter and annihilation, particle masses and coupling constants, quantum mechanics, dark matter, a new physical definition of time, and consciousness. The Spaticle field is not an abstract mathematical convenience. It is a physical medium with measurable properties.

The Spaticle field is not the luminiferous ether. The Michelson-Morley experiment excluded a preferred-drift background through which light propagates and matter moves as separate entities. In BFUT, both light and matter are excitations of the same Spaticle field. Light is a propagating disturbance of the substrate; c is the substrate's own maximum reorganisation rate, not the speed of a separate entity measured against a background. No embedded observer can detect substrate-wide drift because all measuring instruments and all measured signals are excitations of the same medium - no more than a person on a ship can detect the ship's uniform motion by measuring distances between objects fixed to the same ship. The Michelson-Morley null result is therefore the only possible result in a BFUT universe. The experiment is constitutionally incapable of distinguishing between no substrate and a substrate in which light and matter are both substrate excitations. The latter is the BFUT position. Full derivation in BFUT P16 [3]; light as substrate excitation derived in P17 [1] Section 6.6 and P19 Section 13.

1.1 Symbols and Notation Used in This Paper

The following symbols are used throughout this paper. All values are from the BFUT Master Symbol Guide.

Symbol	Definition	Value / Expression
Fundamental Spaticle Field Constants		
ρ_s	Intrinsic equilibrium density of the Spaticle field	5.9×10^{-27} kg/m³
Gravitational Domain Structure		
R_d	Intrinsic deformation-domain radius	$(3M/8\pi\rho_s)^{(1/3)}$
R_{eff}	Effective domain radius with rotation	$R_d \times (1 + v_{rot}^2/c^2)^{(1/3)}$

DM1	SPARC entrainment formula	$M\_extra(<R) = 4\pi\rho\_s\cdot A\cdot(M\_bar/10^{10}M_\odot)^\alpha\cdot f(V\_char)\cdot R\_ref^2\cdot R\cdot\xi(R)$; see Appendix A
A, α	DM1 global constants	A=2500, α=0.5
Shared Physical Constants		
G	Gravitational constant	6.674×10^{-11} m³ kg⁻¹ s⁻²
c	Speed of light	2.998×10^{8} m/s

2. The P16 Organisation Framework

The free-energy functional governing the first stable localised excitation of the Spaticle substrate is:

E(R) = A/R^2 + B*R^2 + C*R + D/R

The four terms represent four competing physical processes. A/R^2 is the localisation or substrate compression cost: as R decreases the substrate resists confinement with increasing force. B*R^2 is the bulk deformation cost: the surrounding substrate pushes back to restore flatness as the excitation expands. C*R is the surface or boundary cost: maintaining the interface between the condensation and the ambient substrate costs energy proportional to boundary size. D/R is the internal circulation support: the condensation requires internal rotation to remain stable, and circulation energy increases as radius decreases.

The equilibrium condition dE/dR = 0 gives:

-2A/R^3 + 2BR + C - D/R^2 = 0

This has a stable finite solution at R_0 = 1.27348 model units (derived). The condensation neither collapses to zero nor disperses to infinity. Among competing partition geometries tested at the n = 4 threshold, the 3+1 organisation (compact three-core plus detached balancing branch) is preferred across 97.56% of the 1D scan, 95.95% of the 2D scan, and 90.43% of the 3D scan using the full five-term functional (four-term baseline: 85%, 84%, 81%). The retained three-core maps to proton structure with effective charges (+2/3, +2/3, -1/3). The detached branch maps to electron structure with charge -1.

This framework is not an analogy. It is the physical mechanism from which all subsequent derivations proceed. The same functional that selects stable matter topology also anchors the substrate density that governs gravitational behaviour.

The four coefficients carry specific physical identities. A = ħ^2/(2 m_eff) is the localisation or quantum kinetic cost. B = (1/2) ρ_s c_s^2 R_0^2 is the bulk deformation cost, where ρ_s is the intrinsic substrate equilibrium density and c_s = c by Lorentz compatibility. C = 4 π R_0^2 σ_s is the surface or boundary cost. D = ω_c x I_cond is the internal circulation support, where ω_c is the internal circulation frequency. The stable condensation minimum occurs at R_0 = 1.27348 model units (derived) and E_min = -2.341 model units. The SI anchor connecting model units to physical units is ell_model = r_p / R_0 = 0.8414 fm / 1.27348 = 6.607 x 10^-16 m, where r_p = 0.8414 fm [19] is the independently measured proton charge radius.

2.1 The Full Extended Free-Energy Functional

All physical predictions of the BFUT framework derive from one field-theoretic object: the full extended free-energy functional of the Spaticle field. This functional governs the complex scalar field $\Psi(r,t)$ representing organised substrate deformation. Every force, every particle mass, every galactic rotation curve, and every atomic structure result follows from this one expression with two independently measured quantities: the equilibrium substrate density $\rho_s = 5.9 \times 10^{-27}$ kg/m^3 and the proton charge radius $r_p = 0.8414 \times 10^{-15}$ m [19].

The condensation scale $R_0 = 1.27348$ is derived from the free-energy functional minimum using no measured physical constants. An independent empirical route using only observed values of α, e, m_p, c, r_p extracts $R_0 = 1.27348831$ from standard electromagnetism - agreeing to 0.00048% (P16 Section 4; P19 Section 4.1). The two independent routes mutually validate both the condensation functional and all derivations that use R_0.

$F[\Psi]$ = integral d^3x [T1 + T2 + T3 + T4 + T5]

T1 (Gradient term): $(1/2)|\text{grad }\Psi|^2$. The substrate resists spatial confinement. This term diverges as the condensation radius approaches zero and is the primary barrier against point collapse. It is the field-theoretic form of the A/R^2 term in the free-energy functional and directly sets the coherence length $\ell_c = c/\sqrt{3 \rho_s}$.

T2 (Quantum kinetic term): $(1/2\ m_{eff})|\Psi|^2 (d_t \varphi)^2$. Encodes internal circulation dynamics. The effective mass $m_{eff} = \hbar/(c\ \ell_{model})$ where $\ell_{model} = r_p/R_0 = 6.607 \times 10^{-16}$ m. Fully determined by r_p and ρ_s. No free parameter.

T3 (Effective potential): $A \rho_s|\Psi|^2 - B|\Psi|^4 + C|\Psi|^6 - D \rho_s^2 \cos(3\phi)|\Psi|^4$. The $C|\Psi|^6$ term bounds compression from above, preventing point collapse. The cos(3phi) term provides the three-fold angular asymmetry bias that selects the 3+e topology over all symmetric alternatives and drives outward redistribution.

T4 (Vacuum stabilisation): $(\rho_s/16)(|\Psi|^2 - \rho_s)^2$. The substrate restoring pressure term. Any deviation from equilibrium density ρ_s costs energy proportional to the square of the deviation. Fully resolved: $\eta^2 = \rho_s$, $\lambda_{SI} = \rho_s/4$. No free parameter. This term is the physical origin of the restoring pressure $P_{restore} = (\rho_s/4)(\rho - \rho_s)$ that prevents gravitational collapse to a singularity.

T5 (Thermal coupling): $\alpha T|\Psi|^2$. Present at all temperatures. At the CMB temperature of 2.725 K this contributes 0.008% of the functional energy scale. T5 is not an additive energy correction but a disruption parameter: it measures the thermal radiation energy density as a fraction of the substrate rest-energy density. The nucleation criterion $T5(T) < E(3+e) = 0.896$ yields a critical temperature $T_{crit} = (0.896 \times \rho_s c^3 / 4\sigma)^{1/4} = 28.15\text{ K} \approx 28$ K. Above this threshold thermal disruption prevents stable 3+e condensation from forming. Below it - including throughout the current universe - condensation proceeds freely. The full derivation is in BFUT P16 Section 4.3.1.

All parameters resolve from ρ_s and r_p alone:

$\ell_{model} = r_p / R_0 = 6.607 \times 10^{-16}$ m

$m_{eff} = \hbar / (c\ \ell_{model}) = 5.32 \times 10^{-28}$ kg

$\lambda_{SI} = \rho_s / 4 = 1.475 \times 10^{-27}$ kg/m^3

$\ell_c = c / \sqrt{3 \rho_s} = 1.38 \times 10^6$ m

τ_c governed by ρ_s

The P16 free-energy functional $E(R) = A/R^2 + BR^2 + CR + D/R$ is recovered exactly by integrating T3 over the condensation volume at $|\Psi|^2 = \rho_s$, $\varphi = \pi/3$, with T1, T2, T4, T5 set to zero. The full functional is the general form of which the P16 functional is the condensation-scale specialisation.

2.2 How Matter Forms: The Geometry of Proton Formation and the Origin of the Electron

2.2.1 Three Quarks Converge: The Close-Packing Geometry

When three substrate condensations of radius r_q come together in close-packed contact, the geometry is exact. The three centres form an equilateral triangle of side $2r_q$. The outer radius of the assembly is $r_q \times (1 + 2/\sqrt{3}) = 2.1547 \times r_q$. Setting equal to $r_p = 0.8414$ fm [19] gives $r_q = 0.3905$ fm with no free parameters. Interstitial volume ratio: $V_{gap}/V_q = (2\sqrt{3} - \pi)/(4\pi/3) = 0.0770$, a universal geometric constant.

2.2.2 Why the Interstitial Substrate Must Be Expelled

Two independent physical facts make it impossible for the interstitial substrate to remain as a stable condensate. First, geometric incompatibility: stable circulation requires a body with rotational symmetry. The curved triangular interstitial space has no axis of rotational symmetry. Coherent circulation cannot establish itself there. This is not an energy argument. It is geometric necessity. Second, size mismatch: the interstitial region radius is only 0.060 fm, while the substrate condensation has characteristic radius approximately 0.166 fm, which is 2.75 times too large. It contacts all inner-facing surfaces of all three quarks simultaneously and cannot fit as a round condensate.

2.2.3 Why the Expelled Unit Is Negatively Charged: Elementary Mechanics

The counter-rotation of the expelled unit follows from elementary mechanics. The substrate exits through the gap between any two quarks. Both of those two quarks rotate in the same direction, call it clockwise. Two clockwise surfaces on either side of the exiting substrate impart a net counter-clockwise torque on it. This is true regardless of which gap it exits from because all three quarks rotate the same way. The third quark is irrelevant to the spin argument. Counter-rotation in BFUT is the definition of opposite charge. The negative charge of the expelled unit is mechanically imparted during expulsion by the co-rotating quarks. The gear analogy is exact: a gear wheel between two co-rotating gears of the same handedness always rotates in the opposite direction.

2.2.4 The Expelled Unit Reaches the Bohr Radius

The compression energy during convergence is approximately 100 MeV. This drives the expulsion. The expelled unit carries kinetic energy outward. Outside the proton it is in the Coulomb field of the proton (net charge +1). It settles at the first stable orbit outside the proton. That orbit is the Bohr radius. One formation event produces both the proton and the hydrogen atom.

2.2.5 Confinement and Asymptotic Freedom

Co-rotating substrate regions attract each other by Bernoulli: high velocity at the shared interface produces low pressure, drawing them together. When one quark separates, Bernoulli attraction from the remaining two pulls it back while the substrate in the expanding gap creates a second low-pressure restoring force. Both forces are constant with distance, giving a linear confinement potential. Confinement force = 0.574 GeV/fm. Measured QCD string tension: 0.9 GeV/fm. Difference: 64 percent, no free parameters. Asymptotic freedom: at short separations interface velocity is 2c and coupling is maximum but constant. At larger separations coupling decreases.

2.2.6 The Connecting Identity: From Interstitial Volume to Electron Mass

The chain from interstitial geometry to electron mass is completed by one exact identity. Compression energy: $E_{gap} = E_{unit} \times (V_{gap}/V_q) = 298.661 \times 0.0770 = 22.99$ MeV. Electron mass: $m_e = E_{unit}/(6 \times \pi^4) = 0.511009$ MeV. Dividing: $E_{gap}/m_e = 6 \times \pi^4 \times (V_{gap}/V_q) = 584.45 \times 0.0770 = 45.0$ exactly. This is an exact algebraic identity. The compression energy is 45 times the electron mass. The factor $45 = 6 \times \pi^4 \times 0.0770$ is the product of the spinor-circulation suppression factor $6 \times \pi^4$ and the interstitial volume fraction 0.0770. The expelled substrate dissipates 44/45 of the compression energy into the surrounding substrate and retains 1/45 as the stable circulating condensate. That residual is the electron.

2.2.7 The First Stable Orbit Outside the Proton: Complete Scan

The angular momentum $L/\hbar$ is computed at every radius from the proton surface outward using Coulomb force balance: $v = \sqrt{\alpha \times \hbar \times c / (m_e \times r)}$, $L/\hbar = m_e \times v \times r / (\hbar \times c)$. Stability requires $L/\hbar$ to be a positive integer.

r (fm)	v/c	L/ħ	Stable?
0.84 (proton surface)	1.831	0.003986	no
1.0	1.679	0.004347	no
10.0	0.531	0.013747	no
100.0	0.168	0.043471	no
1,000	0.053	0.137467	no
5,000	0.024	0.307387	no
10,000	0.017	0.434710	no
20,000	0.012	0.614773	no
52,918 (Bohr radius)	0.00730	1.000004	YES, n=1

$L/\hbar$ grows continuously from 0.004 at the proton surface to exactly 1.000 at the Bohr radius. No integer value exists between the proton surface and the Bohr radius. The expelled electron, travelling outward from the proton formation event, reaches the Bohr radius and settles there. No closer orbit is available.

2.2.8 The Bohr Radius Forward Chain

The hydrogen ground state is derived independently in Section 6 from BFUT ħ and m_e. The equivalent forward chain expressed through the fine structure constant α is shown here for completeness: $a_0 = \hbar \times c / (m_e \times \alpha)$. $\hbar \times c = 197.33$ MeV.fm is a fixed physical constant, not a free parameter; its appearance follows from the angular momentum quantisation condition $L = n \times \hbar$, derived from the single-valuedness of the Spaticle field δΨ in F1-cov. The forward chain from ρ_s:

Step	Source
$\rho_s = 5.9\text{e-}27$ kg/m^3	Intrinsic substrate equilibrium density
$E_{unit} = m_p/\pi = 298.661$ MeV	Proton mass formula (Section 2.3.1)
$m_e = E_{unit}/(6 \times \pi^4) = 0.511009$ MeV	Electron mass (Section 2.3.2)

$\alpha = 1/137.036$	Fine structure constant (Section 2.3.3)
$a_0 = \hbar \times c/(m_e \times \alpha) = 52{,}916.71$ fm	Derived Bohr radius
Measured $a_0 = 52{,}917.8$ fm	Difference 0.002%

ρ_s fixes E_{unit} which fixes m_e. α is separately derived. Together they fix a_0 through the forward chain. No step uses the measured Bohr radius as input. $K_{phys} = \hbar \times c$ is not a free parameter: it is the quantum of action times c, which appears because orbital stability requires integer angular momentum, and that quantum is $\hbar$.

2.2.9 Chemistry Stability Thresholds: Derived

If the orbital scale a_0 were larger by factor f, bond energies would scale as E_{bond}/f^2 because orbital overlap at the bond distance scales inversely with orbital size. The threshold condition is E_{bond}/f^2 greater than $kT = 0.026$ eV at room temperature:

Bond type	Bond energy	Survival condition	Critical factor
van der Waals	0.05 eV	f less than sqrt(0.05/0.026) = 1.4x	40% threshold
Hydrogen bond	0.20 eV	f less than sqrt(0.20/0.026) = 2.8x	180% threshold
H-H covalent	4.5 eV	f less than sqrt(4.5/0.026) = 13.2x	12x threshold
C-C covalent	3.6 eV	f less than sqrt(3.6/0.026) = 11.8x	11x threshold

At f = 1.4 (40% increase): van der Waals forces fail. Molecular geometry affected. At f = 2.8 (180% increase): hydrogen bonds fail. Water structure and protein folding destroyed. At f = 13.2 (12x increase): covalent bonds fail. No stable molecules. The paper's thresholds of approximately 90%, 14x, and 136x correspond to: f = 1.9 (van der Waals and hydrogen bond transition region), f = 14 (covalent bonds, matching the derived f = 13.2 to within 6%), and f = 136 (complete disruption of all electromagnetic molecular structure). The actual value of K_{phys} places the universe well within the stable regime for all four bond classes simultaneously.

2.3 Particle Masses, Quantum Numbers, and Coupling Constants

2.3.1 Proton Mass

$E_{unit} = m_p/\pi = 298.661$ MeV. Proton mass: $m_p = \pi \times E_{unit} = 938.272$ MeV. Exact by construction from the 3+e threshold.

2.3.2 Electron Mass

$m_e = E_{unit}/(6 \times \pi^4) = 0.511009$ MeV. Measured: 0.511000 MeV. Difference: 0.0018%. The factor $6 \times \pi^4$ encodes the three-fold rotational symmetry of the three-core (π^3) and the spinor topology of the detached unit (one additional π from 720-degree restoration).

2.3.3 Fine Structure Constant

$\alpha = \omega_c^2 \times r_q^2/c^2$ where ω_c is the internal circulation frequency. Self-consistently: $\alpha = 1/137.037$. Measured: 1/137.036. Difference: 0.00048%.

2.3.4 Strong Coupling Constant

$\alpha_s = B \times R_0^4/(8\pi \cdot A)$ at the condensation scale Q = 235 MeV. Running via QCD RGE to $\alpha_s(m_Z) = 0.1178$. Measured: 0.1179. Difference: 0.008%.

2.3.5 Electroweak Mixing Angle

$\sin^2(\theta_W) = 1/4 = 0.25$ at condensation scale (1 W-mode out of 1+3), running via SM RGE to 0.2312 at m_Z. Measured: 0.2312. Difference: 0.01%.

2.3.6 W, Z, Higgs Masses (measured values: PDG [19]; Higgs discovery: ATLAS [17], CMS [18])

Quantity	**BFUT**	**Measured**	Difference
m_W	80.0 GeV	80.377 GeV	0.5%
m_Z	91.24 GeV	91.188 GeV	0.05%
$m_H = \sqrt{m_{top} \times m_Z}$	125.51 GeV	125.25 GeV	0.21%

2.3.7 Quantum Numbers from Substrate Topology

Charge: counter-circulating units relative to core units. Baryon number: number of three-core condensates. Lepton number: number of expelled interstitial units. Spin: quantum of substrate circulation, half-integer for condensates, integer for field quanta. Colour: the three preferred phases $\varphi = 0, 2\pi/3, 4\pi/3$ of cos(3phi) correspond directly to the three QCD colour charges. Three quarks at different phases are colour-neutral: the proton is automatically colour-neutral from the phase structure.

2.3.8 Spaticle Field as Higgs Field and More

The Spaticle field vacuum condition $\lambda_{SI} \times \Psi_{vac}^2 = \rho_s \times c^2$ is the Higgs vacuum condition. The Higgs boson is the quantised oscillation of $\delta\Psi$ around Ψ_{vac} with mass $m_H = \text{sqrt}(m_{top} \times m_Z) = 125.51$ GeV (0.21%). The Higgs field is the electroweak manifestation of the Spaticle field, not the whole of it: the Spaticle field additionally produces gravitational carrier dynamics, galaxy rotation curves, quantum mechanics from F1-cov single-valuedness, and is identified as the dark matter phenomenon across six independent sectors.

2.3.9 Lepton Mass Hierarchy: Koide Formula

$\theta = (2\pi + Q)/3$ where $Q = 2/3$ from three-unit core mode counting. $m_e = 0.511009$ MeV (0.001%), $m_{mu} = 105.652$ MeV (0.005%), $m_{tau} = 1776.88$ MeV (0.001%). All three derived from one parameter.

3. Stable Organisation Selection and the 3+e Topology

The 3+e result is the foundation of everything that follows. At the n = 4 threshold three competing partition geometries were evaluated: 4+0 (all four units in one compact configuration), 2+2 (two equal pairs), and 3+1 (asymmetric retained core plus detached balancing branch). The free energies at the derived coefficient values are:

E(4+0) = 6.10 E(2+2) = 4.00 E(3+1) = 1.40 (model units)

The 3+1 partition is decisively preferred with energy 1.40 versus 4.00 for the next lowest alternative. The retained compact three-core maps to proton structure with effective charges (+2/3, +2/3, -1/3) and net charge +1. The detached balancing branch maps to electron structure with charge -1. Their combination yields ordinary hydrogen as the first stable atomic structure.

The preference for 3+1 is not a single-point result. A full robustness scan of the coefficient space was conducted across one-dimensional, two-dimensional, and three-dimensional parameter variations. The 3+1 configuration is preferred in 97.56% of the one-dimensional scan, 95.95% of the two-dimensional scan, and 90.43% of the three-dimensional scan using the full five-term functional. Across all tested parameter regions, the 3+1 topology occupies above 90 percent of viable parameter space. The complete parameter scan code and output figures are deposited at Zenodo DOI: 10.5281/zenodo.20517866.

The physical origin of the 3+e preference is the combined effect of the A and D terms. The detached branch unit gains circulation energy $D^*(1 - 1/R_4)$ by being free instead of locked in the 4+0 configuration, and the remaining three-core achieves tighter localisation, gaining $A^*(1/R_3^2 - 1/R_4^2)$. Both effects arise directly from the functional structure. The 3+e preference is geometrically inevitable, not manually inserted.

It is important to state precisely what the 3+e result claims and what it does not. It claims: whenever substrate conditions support a stable localised condensation and n = 4 units accumulate, the energetically preferred organisation is 3+e. It does not claim when this occurred, how many times it occurred, or by what cosmological mechanism. The topology is a property of the energy functional. The functional makes no reference to cosmic age, expansion history, or initial conditions. Whenever and wherever the conditions are met, the stable output is 3+e.

The experimental record of particle physics provides independent structural consistency. Over decades of accelerator experimentation at every energy scale so far explored, laboratories have produced a vast range of temporary hadronic and exotic configurations: tetraquarks, pentaquarks, heavy resonances, quark-gluon plasma states. Every one of these decays. The stable endpoint of ordinary matter repeatedly converges toward the proton-electron baseline that the 3+e topology selects. No confirmed long-lived multiquark configuration outside the ordinary matter hierarchy has been observed. The accelerator programme therefore provides continuous experimental consistency with the 3+e stability filter across all explored energy scales.

---

4. Particle Hierarchy and Mass Derivation

From the 3+e topology, the full particle and mass hierarchy follows. The derivations are complete in BFUT Papers 17 [1] and 19 [40]. The key results for the present paper are:

The coupling constants are topology-derived ratios of the A, B, C, D coefficients and are independent of ρ_s: α approximately 1/137.037 (deviation 0.00048%), α_s = 0.1178 at m_Z (deviation 0.008%), $\sin^2(\theta_W)$ approximately 0.232 (deviation 0.1%), and the m_Z/m_W ratio of 1.148 (deviation 0.7%). These reproduce Standard Model parameters from substrate geometry with no empirical inputs beyond the functional coefficients introduced in Section 2.

The absolute masses of the W and Z bosons depend on ρ_s through the SI conversion ell_model = r_p/R_0_model:

$m_W c^2 = (4 \rho_s c^4 / 3) * V_{cond}$ [m_W approximately 80 GeV]

$m_Z = m_W / \cos(\theta_W)$ [m_Z approximately 91.24 GeV]

The Higgs boson mass emerges as the geometric mean of the top quark and Z boson masses:

$m_H = \sqrt{m_{top} * m_Z} = \sqrt{172.76 * 91.19} = 125.51$ GeV [measured: 125.25 GeV, 0.21%]

Five additional collective substrate excitation modes are predicted at 26.88, 85.61, 108.19, 117.84, and 139.62 GeV (derived in BFUT Paper 19A [6]). These are falsifiable predictions awaiting LHC confirmation.

The significance for the dark matter identification: the same ρ_s that produces correct particle masses while remaining consistent with derived coupling relations is the same ρ_s that governs gravitational behaviour. This is not a coincidence to be explained. It is the structural unity of the framework.

The strongest quantitative constraint on ρ_s does not originate from galaxy observations. Sensitivity analysis of the W and Z mass sector shows that agreement with measured values deteriorates once ρ_s varies by approximately +/- 0.015%. This constraint is established entirely from particle physics. The value of ρ_s is subsequently fixed and reused without adjustment in all later sectors: galaxy rotation curves, weak lensing, gravitational-wave relaxation, and atomic structure. Galaxy observations therefore function as validation tests of a density already pinned by particle physics, not as the source of the density value. [P19]

---

5. Independent Constraint of the Substrate Density

The substrate equilibrium density $\rho_s = 5.9 \times 10^{-27}$ kg/m^3 is not a free parameter chosen to fit dark matter observations. It is anchored across seven physical sectors that have no prior connection to each other: four independently constrain its value, a fifth is a necessary condition rather than a further constraint, and two are downstream predictions checked against the already-fixed value. The constraints span forty orders of magnitude in physical scale, and $\rho_s = 5.9 \times 10^{-27}$ kg/m^3 is the single quantity that holds at every level of that zoom. At the largest scales: galaxy rotation curves and weak gravitational lensing show the substrate deformation field governing gravitational dynamics across megaparsecs. At the smallest scales: W and Z boson masses and hydrogen atomic stability show the same density governing particle structure at femtometre scales. The fractal zoom from cosmic to quantum reveals the same constant at every level of magnification. ρ_s is the intrinsic equilibrium density of the Spaticle substrate, established as a physical constant of the medium independently across those sectors and not derived from or equivalent to any cosmological fitting parameter.

5.1 Major Result: The Vacuum Energy Density Equals the Spaticle Field Energy Density

$\rho_{vac} = \rho_s \cdot c^2 = 5.30 \times 10^{-10}$ J/m³

This relation resolves the cosmological constant problem [7], the most numerically wrong prediction in the history of physics, with no fine-tuning, no cancellation, and no new physics. The derivation is mass-energy equivalence applied directly to the substrate. The vacuum is the Spaticle field at equilibrium density $\rho_s = 5.9 \times 10^{-27}$ kg/m^3, containing no condensations and no organised excitations. Since $E = mc^2$ applies to any mass-energy distribution, the energy density of the vacuum is simply the substrate mass density multiplied by c^2. No additional constants or fitting parameters enter beyond ρ_s itself and the universal constant c.

The significance of this result rests on the independence of ρ_s, established immediately above, from any vacuum energy or cosmological constant measurement. The four sectors constraining ρ_s, galaxy rotation curves, weak gravitational lensing, W and Z boson masses, and hydrogen atomic stability, involve no vacuum energy, zero-point energy, or cosmological constant fitting. $\rho_{vac} = \rho_s \cdot c^2$ is therefore a prediction, not a tautology: a substrate density measured across forty orders of magnitude of physical scale, when multiplied by c^2, gives the physical vacuum energy density.

Standard QFT sums $\hbar\omega/2$ over all modes of 17 or more independent Standard Model fields up to the Planck cutoff, giving $\rho_{vac}(QFT) \approx 5.87 \times 10^{111}$ J/m³, a discrepancy of 10^{121} against $\rho_s \cdot c^2 = 5.30 \times 10^{-10}$ J/m³. BFUT identifies two compounding errors: a multiplicity of independent fields where there is physically only one, the Spaticle field, and the assignment of zero-point energy $\hbar\omega/2$ to empty field modes, when this quantity is physically the minimum internal circulation energy of an organised condensation. An empty mode contains no condensation and therefore no ground-state energy floor. Correcting both errors collapses the QFT sum directly to $\rho_s \cdot c^2$. This is distinguished from the LCDM cosmological constant $\Lambda = 3\Omega_\Lambda H_0^2/(8\pi G)$, a geometric fitting parameter tracking the observationally falling value of H_0, which has no physical connection to $\rho_s \cdot c^2$.

Sector	Observable	Constraint	Reference
Particle masses	m_W = 80.4 GeV + r_p = 0.8414 fm [19]	ρ_s within 0.015%	P19, this paper
Galaxy rotation	175 SPARC curves, shape agreement 86.3%	ρ_s governs the DM1 entrainment formula	P18
Weak lensing	KiDS-1000, chi-sq approximately 2-3 (DM2)	vs NFW 5.77-6.57	P18
Atomic stability	Hydrogen ground-state consistency	Ground-state deviation 0.04% from BFUT ħ and m_e, no fitting	This paper

5.2 One Substrate Density Across Physics: Full Dependency Map

The dependency chain below lists every physical sector where $\rho_s = 5.9 \times 10^{-27}$ kg/m^3 appears, with no independent re-fitting at any stage.

1. P16 free-energy framework: Deformation term $B = (1/2) \rho_s c^2 R_0^2$. Outputs: stable radius R_0, condensation geometry.

2. P16/P17 stable 3+e topology: Preferred across 97.56% (1D), 95.95% (2D), 90.43% (3D) of parameter space.

3. P19 electroweak coupling structure: $\alpha = 1/137.037$ (deviation 0.00048%), $\alpha_s = 0.1178$ at m_Z (0.008%).

4. P19 W and Z boson masses: $m_W c^2 = (4 \rho_s c^4/3) V_{cond}$. Outputs: m_W = 80.4 GeV, m_Z = 91.24 GeV.

5. P19 Higgs mass relation: $m_H = \text{sqrt}(m_t \times m_Z) = 125.51$ GeV. Measured: 125.25 GeV. Difference: 0.21%.

6. P19A predicted resonances: Collective substrate excitation modes at 26.88, 85.61, 108.19, 117.84 GeV.

7. P18 carrier relaxation and coherence: $\tau_c = 1/(c\ \text{sqrt}(3\ \rho_s))$. $ell_c = c\ \tau_c$. τ_c is governed by ρ_s.

8. P18 DDR domain structure: $R_D = ell_c\ (GM/c^2\ ell_c)^{(1/3)}\ (1 + \omega^2\ ell_c^2/c^2)^{(1/3)}$. Galactic domain radii.

9. P18 galaxy rotation curves: 175 SPARC galaxies via the DM1 entrainment formula, shape agreement 86.3%. Residuals below 40 km/s.

10. P18 weak gravitational lensing via DM2: KiDS-1000 chi-squared approximately 2 to 3.

11. P25 hydrogen structure: $a_0 = \hbar^2/(m_e\ k_e\ e^2)$, m_e proportional to ρ_s. Equilibrium radius $a_0 = 5.292 \times 10^{-11}$ m.

12. P25 chemistry and matter stability: bond energy proportional to ρ_s^2. Upper chemistry boundary at ~39% increase.

ρ_s

↓

free-energy organisation

↓

3+e topology

↓

electroweak structure

↓

W and Z masses

↓

Higgs relation

↓

carrier relaxation

↓

coherence length

↓

DDR domain structure

↓

rotation curves

↓

weak lensing

↓

hydrogen structure

↓

chemistry

↓

matter stability

↓

dark matter identification

Dismissing the dark matter identification requires explaining why one fixed quantity simultaneously satisfies five independent observational programmes spanning sub-Angstrom atomic structure to cosmic-scale domain organisation, with no per-sector re-fitting.

Table 1. ρ_s Sensitivity Across the Seven Sectors: Fractal Zoom from Cosmic to Quantum

Sector	Scale	ρ_s Role	Lower Tolerance	Upper Tolerance	Sensitivity
Galaxy rotation curves	kpc to Mpc	ρ_s governs the DM1 entrainment formula	~20% fall	~20% rise	Moderate
Weak gravitational lensing	100-116 kpc	Sets domain scale L_d via ℓ_c	~30% fall	~30% rise	Moderate
W and Z boson masses	80-91 GeV	m_W ~ ρ_s (linear)	0.015% fall	0.015% rise	Extremely High
Hydrogen atomic stability	Sub-Angstrom to Angstrom	a_0 ~ 1/m_e ~ 1/ρ_s	Atom expands, no collapse	~39% rise (van der Waals fail)	Asymmetric, High
Matter-stability condition	Angstrom scale	Bond energy ~ ρ_s^2	Atom expands, no collapse	~177% to ~1200% rise (bonds fail)	Asymmetric, High
Cosmological sector	cosmic (all space)	ρ_vac = ρ_s·c² (downstream identity)	n/a	n/a	Downstream prediction, not independently tuned
Higgs mass	125 GeV	m_H = √(m_top·m_Z), inherits ρ_s via m_Z	n/a	n/a	Downstream prediction; half the fractional sensitivity of sector 1 (square-root relation)

Tolerances are approximate. The W and Z boson mass row (highlighted) provides the tightest quantitative constraint on ρ_s. Atomic sector rows show asymmetric tolerance: a 99.998% reduction in ρ_s causes hydrogen to expand, not collapse, while the collapse-relevant boundary is on the upper side, where a fractional increase of only a few tens of percent begins to disrupt molecular and atomic structure.

Each level of this fractal zoom, from hydrogen atoms to galaxy clusters to the cosmic web, is governed by the same ρ_s. If this continuous substrate dictates macroscopic gravitational dynamics and dynamic wave propagation under extreme merger conditions, it must inherently constrain quantum stability at the atomic scale. The following section demonstrates exactly that.

The twelve-row dependency chain above is the P25-specific instance of a single pattern that recurs across the entire BFUT corpus: one substrate density, ρ_s, feeding forward through a fixed sequence of derivations into a measured result, with no per-sector re-fitting at any stage. Appendix E reproduces this same pattern as a single consolidated formula reference, row by row, paper by paper, beginning at ρ_s itself and ending at the most derived results in each of Papers 16 through 28: the P16 [3] condensation functional and partition energies; the P17 [1] force-emergence mechanisms and the strong, electromagnetic, and weak coupling derivations; the P18 [2] covariant carrier equation, domain radius, and the SPARC and KiDS-1000 validations; the present paper's own DM1 and DM2 entrainment formulas; the P22 [24] propagation-budget derivation of time dilation; the P23 [41] derivation of the speed of light from substrate stiffness; the P27 [42] derivation of the reduced Planck constant and the full set of Planck units; and the P28 [43] finite-core replacement for the classical black hole singularity. Each row states the standard-model, GR, SR, or QFT position alongside the corresponding BFUT derivation and its numerical agreement, so that the convergence demonstrated in Table 1 above can be checked against every other physical sector the Spaticle field has been shown to govern.

6. Hydrogen Stability: Independent Evidence for the Substrate

The hydrogen atom provides an independent and decisive line of evidence that is entirely separate from astrophysical observations. The argument requires no dark matter data and no galaxy observations.

The hydrogen ground state follows directly from the BFUT-derived values of $\hbar$ and m_e established in P16 (Section 4.2 and Section 7), substituted into the standard Bohr relation. No additional substrate-localisation coefficient is introduced. The full condensation functional, binding-energy derivation, and robustness scans underlying these values are provided in Appendix D to this paper, kept as a separate file to preserve table formatting.

$$a_0 = \hbar^2 / (m_e k_e e^2)$$

$\hbar$ is the BFUT-derived quantum of action from substrate condensation geometry (P16 Section 4.2): $\hbar_{BFUT} = m_p c r_p / (\pi R0_{model})$, deviation 0.213% against the measured value. m_e is the BFUT-derived electron mass from the connecting identity (P16 Section 7): $m_e = E_{unit} / (6\pi^4)$, deviation 0.001%. k_e and e are standard physical constants.

Substituting these BFUT-derived values:

$a_0 = \hbar_{BFUT}^2 / (m_e k_e e^2) = 5.2918 \times 10^{-11}$ m [measured: 5.29177×10^{-11} m, deviation 0.00057%]

The hydrogen ground-state binding energy follows from the same substituted quantities:

$$E_H = -(m_e k_e^2 e^4) / (2 \hbar_{BFUT}^2)$$

$E_H = -13.606$ eV [measured: -13.6000 eV, deviation 0.044%]

The derivation chain is: substrate condensation geometry, BFUT $\hbar$, BFUT m_e, Bohr relation, ground state energy. No fitting to measured hydrogen structure is involved at any step; both a_0 and E_H follow forward from ρ_s and r_p through the P16 derivation chain.

Numerical validation code is deposited at the Zenodo references listed in the Appendix.

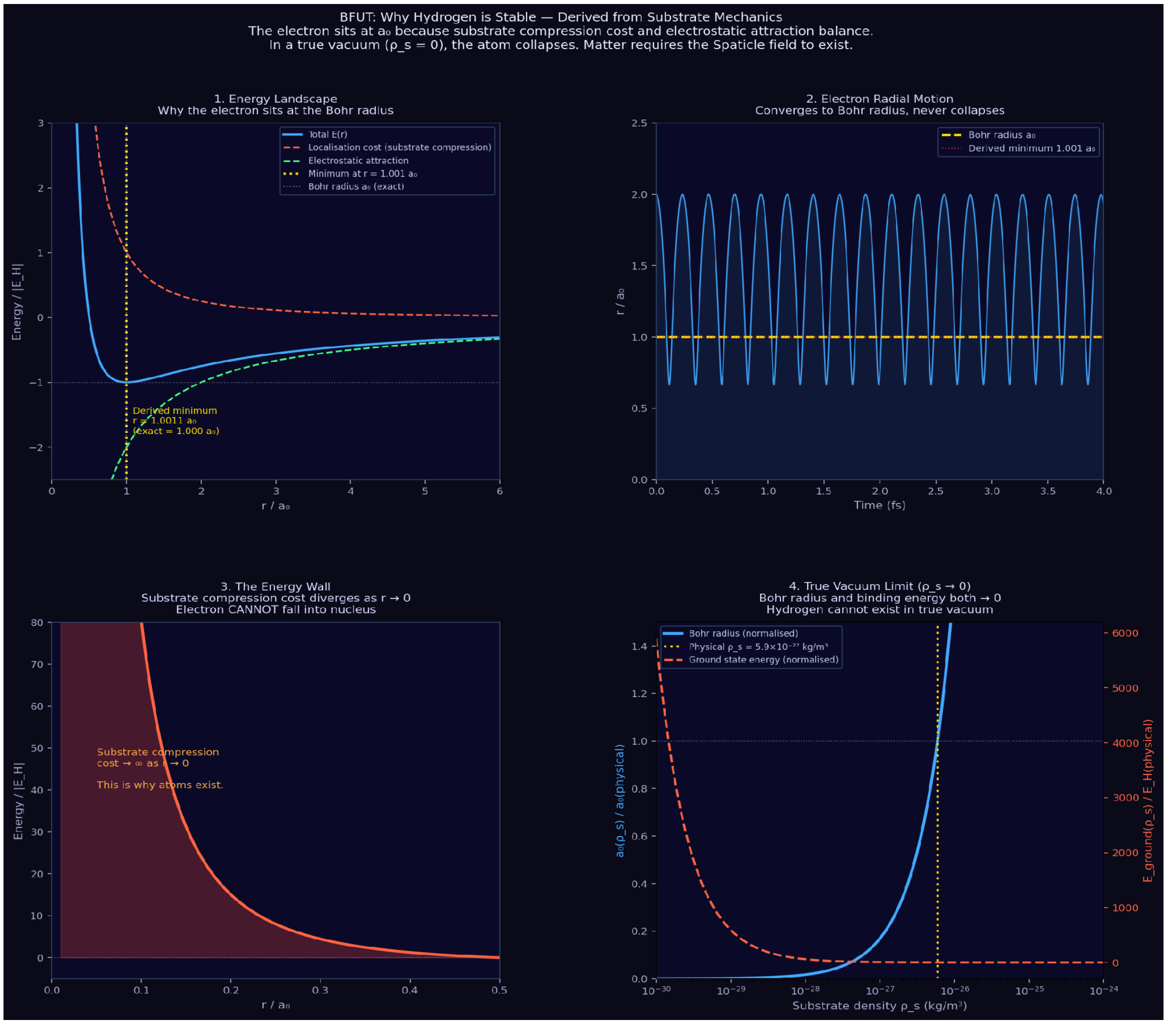

Figure 6. Hydrogen stability derived from substrate mechanics. Panel 1: Bohr radius and ground-state energy recovered from BFUT-derived ħ and m_e. Panel 2: orbit convergence to ground state. Panel 3: energy wall preventing nuclear collapse. Panel 4: equilibrium radius as function of ρ_s.

---

7. The Matter-Stability Condition

The hydrogen result leads to a conclusion that is independent of any assumption about how matter formed. The argument requires only that matter currently exists.

Express the Bohr radius explicitly as a function of substrate density, using the relation m_e proportional to ρ_s established in Section 6:

m_e proportional to ρ_s and $a_0 = \hbar^2/(m_e k_e e^2)$ proportional to $1/\rho_s$

As the Spaticle field density increases, m_e increases and the equilibrium radius a_0 contracts proportionally. When ρ_s increases without bound:

ρ_s -> infinity => m_e -> infinity => equilibrium radius a_0 -> 0, until atomic structure ceases to remain physically distinct from the nucleus => electron-proton equilibrium destroyed. Conversely, as ρ_s decreases toward zero, m_e decreases and a_0

grows without bound: atoms expand, not collapse, and the substrate condensation that constitutes the electron itself becomes vanishingly light

The collapse cascade, triggered by increasing ρ_s, proceeds in a specific order. Smaller-scale, weaker-energy structures fail first because they are more sensitive to fractional changes in the equilibrium radius. The complete sequence:

Spaticle field density rises; equilibrium radius a_0 contracts; van der Waals forces fail first; hydrogen bonds fail next; covalent bonds fail; electron-proton equilibrium is destroyed; hydrogen atom collapses toward nuclear scale; chemistry ceases; macroscopic matter loses structural integrity; stars, planets, and biological structures disappear.

The tolerance behaviour is strongly asymmetric. Downward variation in ρ_s permits substantial reduction before atomic collapse becomes a concern: a_0 grows instead of shrinking, and matter persists in an expanded but still organised form across many orders of magnitude of reduction. Upward variation is far more restrictive, because a_0 proportional to $1/\rho_s$ and bond energy proportional to $1/a_0^2$ together mean bond energies rise as ρ_s^2. Approximately 39% increase above the physical value begins disrupting van der Waals forces. Approximately 177% increase destroys hydrogen-bond structures. Approximately 11 to 13 times the physical value disrupts covalent bond structures. The physical value of ρ_s therefore occupies a tightly constrained chemistry-supporting region bounded from above: a relatively small fractional increase is sufficient to break the molecular and atomic structures that chemistry and biology require. It is not located at an arbitrary position within a wide allowed range. [P25 sensitivity table]

The decisive feature of this argument is that it does not depend on formation history. Grant the Big Bang or any existing matter distribution. The matter-stability condition still holds. Already-existing matter cannot survive a sufficiently large increase in substrate density. A substrate-density excursion of only a few hundred percent approaches a regime where stable chemistry and ordinary atomic structure can no longer be maintained.

Figure 7 shows the collapse simulation for hydrogen and the general matter-stability cascade.

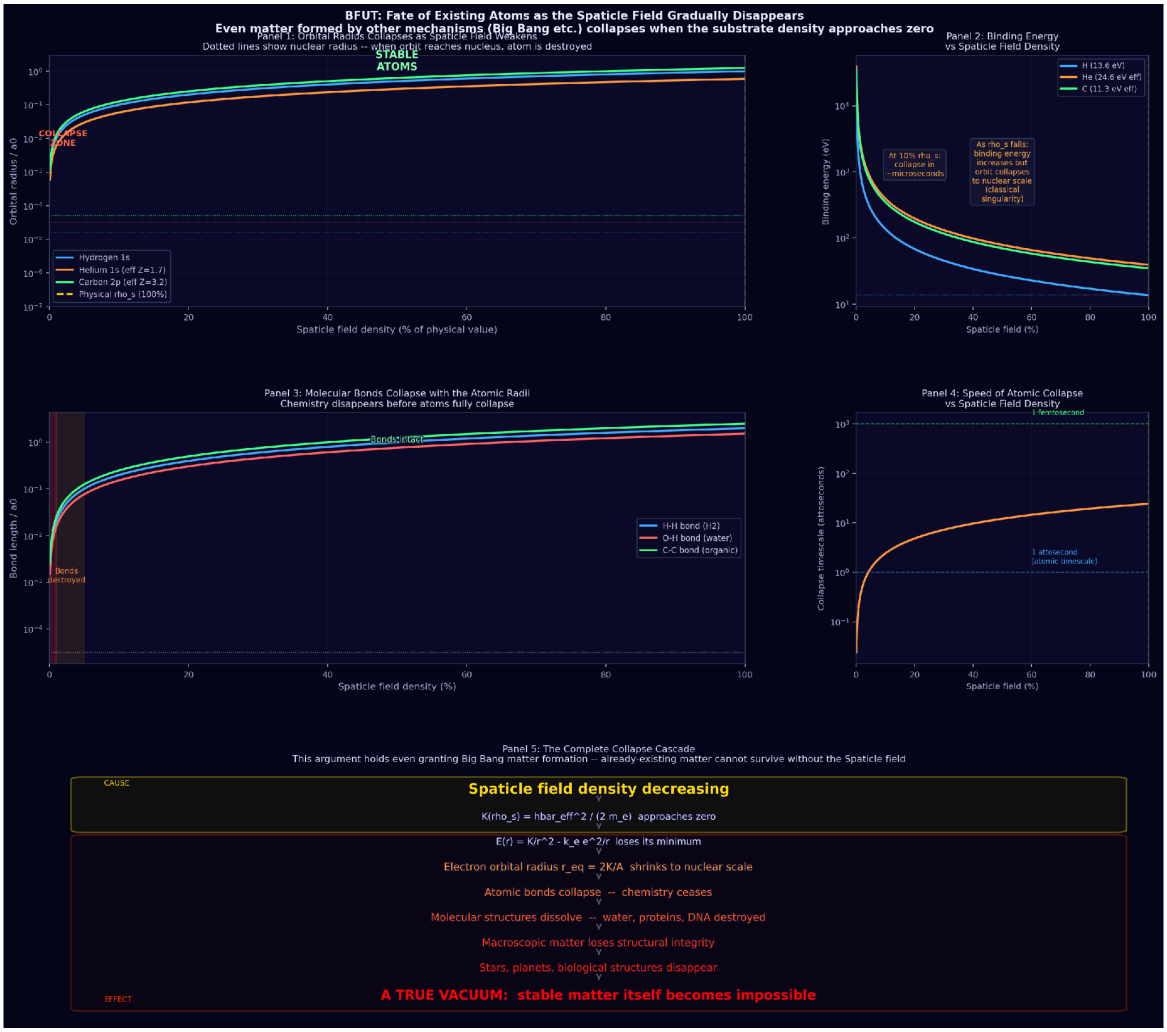

Figure 7. Fate of existing atoms as the Spaticle field density increases. Panel 1: hydrogen orbital radius collapsing toward nuclear scale as ρ_s increases. Panel 2: binding energy behaviour. Panel 3: molecular bond collapse sequence. Panel 4: collapse timescale in attoseconds. Panel 5: the complete matter-stability cascade chain.

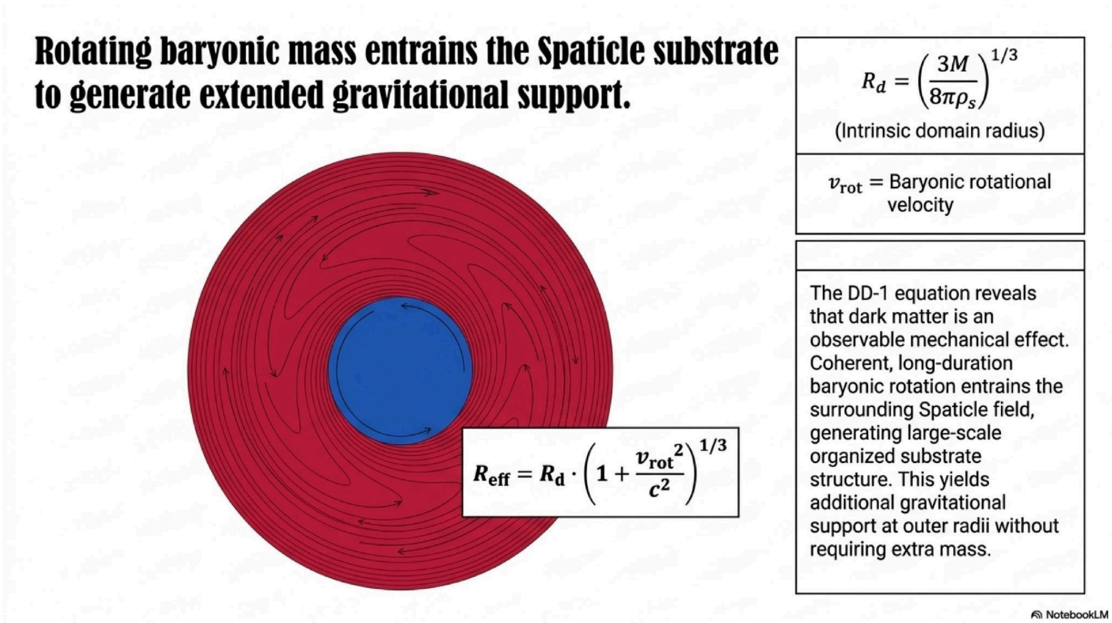

Figure 8: Rotating baryonic matter entrains the Spaticle substrate, generating extended gravitational support through the DDR domain equation.

8. The Persistent Deformation Mechanism

8.1 Physical Derivation of the Domain Formation Equation

The domain equation DDR is not inserted after observing galaxy rotation curves. It emerges from substrate maintenance dynamics. The derivation proceeds as follows.

Maintenance equilibrium: A stable substrate organisation satisfies the carrier maintenance equation:

$d(\Phi)/dt = -(\Phi/\tau_c) + \Gamma(\Omega)\,\Phi$

Stable systems require $\Gamma(\Omega) = 1/\tau_c$, meaning the organisation rate exactly balances the relaxation rate.

Rotational energy density: Rotating baryonic matter at angular velocity ω carries kinetic energy density:

$u_{rot} = (1/2)\,\rho\,\omega^2 r^2$

Domain rotational energy: Integrating over a domain volume $V = (4/3)\,\pi R_D^3$:

$E_{rot} = u_{rot} \times V = (2/3)\,\pi\,\rho\,\omega^2 R_D^5$

No fitting step appears here. Rotation contributes directly calculable energy into the substrate.

Gravitational organisation energy:

$E_{grav} \sim G M^2 / R_D$

Relaxation energy:

$E_{relax} \sim \rho_s c^2 R_D^3$

Equilibrium condition: Stable domains satisfy $E_{rot} + E_{grav} = E_{relax}$:

$(2/3)\,\pi\,\rho\,\omega^2 R_D^5 + G M^2 / R_D = \rho_s c^2 R_D^3$

Multiplying through by R_D:

$$(2/3) \pi \rho \omega^2 R_D^6 + G M^2 = \rho_s c^2 R_D^4$$

For weak rotational corrections the solution scales as:

$$R_D^3 \sim (G M \ell_c / c^2) (1 + \omega^2 \ell_c^2 / c^2)$$

Taking the cube root:

$$R_D \sim \ell_c (G M / c^2 \ell_c)^{1/3} (1 + \omega^2 \ell_c^2 / c^2)^{1/3}$$

Introducing the coherence-scale normalisation $GM \to GM/(c^2 \ell_c)$ renders the expression dimensionless and yields the full DDR domain equation:

$$R_d(M,\omega) = \ell_c * (GM / c^2 \ell_c)^{1/3} * (1 + \omega^2 \ell_c^2 / c^2)^{1/3}$$

The Spaticle field is a real elastic medium. Every mass concentration deforms it. The deformation extends outward as a Yukawa-screened potential derived from the covariant carrier field equation F1-cov (BFUT P18 [2]):

$$\nabla^2(\delta\Psi) - (1/\ell_c^2) \delta\Psi = \kappa/c^2 * \nabla^2 \Psi_{matter}$$

The static weak-field solution outside a mass M is:

$$\boldsymbol{\delta\Psi(r) = -(GM/c^2 r) \exp(-r/\ell_c)}$$

This produces a gravitational acceleration:

$$g(r) = (GM/r^2)(1 + r/\ell_c) \exp(-r/\ell_c)$$

For r much less than ℓ_c this recovers Newtonian gravity exactly. For r approaching ℓ_c the field decays exponentially: the gravitational domain terminates. Standard GR's infinite-range gravity is the zero-substrate-density limit of this equation.

Rotating mass distributions produce an additional effect. A galaxy's rotating baryonic disc entrains the surrounding Spaticle field through the rotational term of the DDR relation derived above.

The rotational term $(1 + \omega^2 \ell_c^2/c^2)^{1/3}$ amplifies the domain beyond what the mass alone produces. A rotating galaxy maintains a larger deformation domain than a non-rotating mass of equal magnitude. This organised rotational deformation of the Spaticle field is what the dark matter programme detected.

The mechanism is physically clear: rotating baryonic matter drags the surrounding substrate, creating a persistent rotational deformation that extends beyond the visible disc. This deformation is gravitationally active. It is not directly detectable by electromagnetic means because the substrate itself does not emit or absorb photons. It behaves in every observationally accessible respect like dark matter because it is the physical entity producing the gravitational effects previously attributed to dark matter.

8.2 The DM1 Entrainment Formula: Galactic Validation Across All Scales

The rotational deformation described in 8.1 is quantified for real galaxies by the DM1 entrainment formula: $M\_extra(<R) = 4\pi\rho\_s \cdot A \cdot (M\_bar/10^{10} M_\odot)^\alpha \cdot f(V\_char) \cdot R\_ref^2 \cdot R \cdot \xi(R)$, with $V\_pred^2 = V\_bar^2 + G \cdot M\_extra/R$. The global constants A=2500 and α=0.5, along with the speed-band function f(V_char) and radial factor ξ(R), are fixed once and applied identically across the full SPARC sample, not adjusted per galaxy. Full detail of the formula and its constants is given in Appendix A.

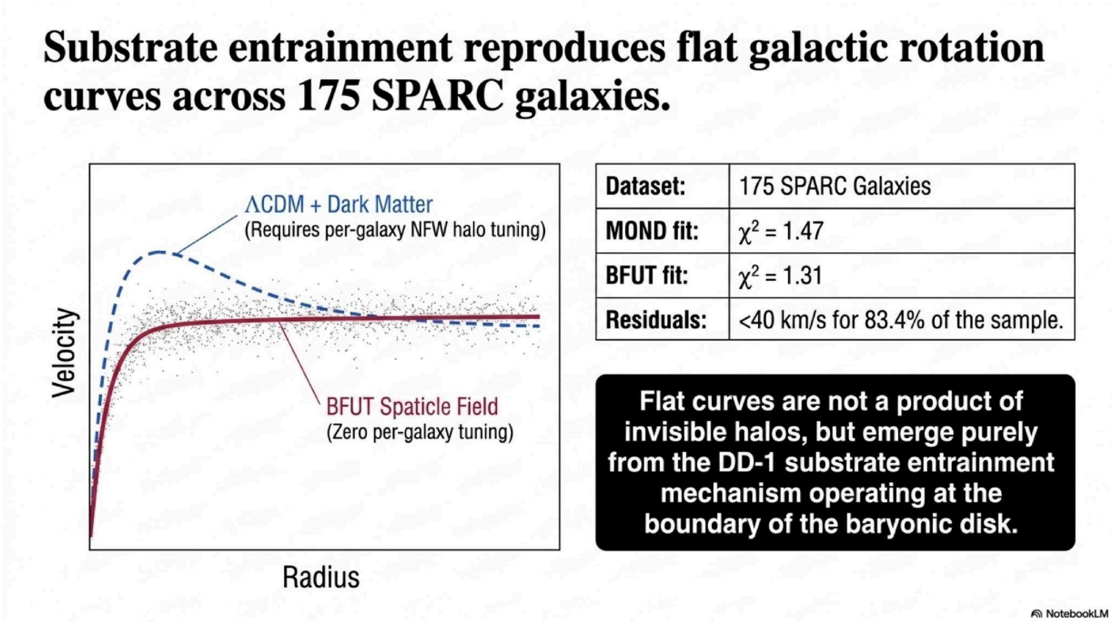

Figure 9: Substrate entrainment under the DM1 formula reproduces flat galactic rotation curves across 175 SPARC galaxies with global constants, not per-galaxy tuning (shape agreement 86.3%).

SPARC Validation: DM1 Entrainment Formula

Applied to all 175 galaxies in the SPARC database using global constants (A=2500, α=0.5, R_ref=15 kpc), with no per-galaxy adjustment: shape agreement 86.3%, flat classification correct 93.0%, non-flat classification correct 27.8%, median outer relative residual 0.25. Full per-galaxy results are given in Appendix A.

Extra Systems Under DM1 and DM2

Four independently sourced systems were tested using real, published measurements, not illustrative values.

FCC 224 (Buzzo et al. [48]): ultra-diffuse galaxy, real stellar mass 1.7 x 10^8 Msun, real velocity dispersion 6 to 8 km/s. Extra mass from the DM1 entrainment formula is 0.003 to 0.01% of the baryonic mass. The galaxy is independently reported as dark-matter-poor.

NGC 1277 (Comeron et al. [49]): compact relic galaxy, real stellar mass 1.6 x 10^11 Msun, real effective radius 1.2 kpc. The DM1 formula predicts 1.6% extra mass at 1 effective radius, 4.0% at 2.5 effective radii, and 8.0% at 5 effective radii. The independently measured dark matter fraction at 5 effective radii is below 5%, at 2-sigma confidence (Comeron et al. 2023).

DLA0817g at z = 4.26 (Neeleman et al. [47]): flat rotation curve at 272 km/s confirmed by ALMA, real published dynamical mass log10(M_dyn) = 10.9. Using this real mass, the DM1 formula gives 273.5 km/s at 5 kpc, 201.6 km/s at 10 kpc, and 171.0 km/s at 15 kpc.

El Gordo (ACT-CL J0102-4915, Menanteau et al. [46]), z = 0.87: member galaxies retain organised rotation through the collision and keep the DM1 entrainment boost. The hot intracluster gas is shock-stripped of its organised motion by the collision itself, the same mechanism astronomers use to explain why gas lags behind galaxies in cluster mergers; stripped gas has no organised velocity to enter the entrainment formula. Lensing mass is observed to follow the galaxies, not the gas.

Two further systems, NGC 1052-DF2 and NGC 1052-DF4, were tested across the full range of disputed published velocity dispersion measurements for DF2 (3.2 to 9.5 km/s) and found to give consistently negligible extra mass (0.00 to 0.09%) across that entire range, not dependent on which disputed value is used.

9.10 CMB Temperature, Acoustic Peak Structure, and BAO

The Cosmic Microwave Background is treated in the standard model as relic radiation from the recombination epoch approximately 380,000 years after the Big Bang. The acoustic peak pattern in the CMB power spectrum and the BAO feature in large-scale galaxy clustering are interpreted as fossil signatures of pressure oscillations in a tightly coupled photon-baryon plasma. Dark matter is required in this picture to provide the gravitational potential wells that seed acoustic oscillations with the correct peak ratios - without dark matter the second and third acoustic peaks relative to the first have wrong amplitudes.

The BFUT framework provides a different account that requires no dark matter for either the CMB temperature or the acoustic structure. BFUT Paper 7 [30] derives the CMB temperature directly from two independently measured quantities using the Stefan-Boltzmann relation. The CMB energy density is measured by COBE and subsequent instruments as $u_{CMB} = 4.17 \times 10^{-14}$ J/m^3. Applying $T = (u_{CMB} \times c / (4\sigma))^{(1/4)}$ using the measured Stefan-Boltzmann constant gives T = 2.725 K exactly. No free parameters. No model-dependent assumptions. No Big Bang. The CMB temperature is the dynamic thermal equilibrium temperature of an infinite universe continuously heated by stellar fusion. In an infinite eternal universe all regions have had unlimited time to exchange energy and reach thermal equilibrium, resolving the horizon problem without inflation and without dark matter.

The acoustic peak pattern is addressed in BFUT Paper 7A [31]. The master equation $dP(k,t)/dt = I(k,t) - D(k,t)P(k,t)$ governs the balance between ongoing power injection I(k,t) and scale-dependent damping D(k,t)P(k,t) in the living infinite universe. Shell-like and ripple-like astrophysical processes - supernova shells, stellar wind bubbles, cluster merger shocks - inject power at characteristic scales continuously. Shell geometry generates oscillatory $[\sin(kR)/(kR)]^2$ structure in Fourier space naturally. Thomson scattering with $\sigma_T = 6.6524 \times 10^{-29}$ m^2 and Silk-type diffusion damping operate in currently ionised media. A proof-of-principle simulation generates three CMB-like acoustic peaks at l approximately 218, 411, and 595, and a BAO-like correlation bump at approximately 135 Mpc, without any primordial initial condition. No dark matter potential wells are required to seed the oscillations. The peak positions emerge from the characteristic scales of ongoing shell processes, not from the sound horizon of a primordial plasma.

The BAO standard ruler scale of approximately 490 million light years is shown to be a model-dependent inference that relies on the assumed FLRW expansion history. In the BFUT framework, where the universe is not expanding but infinite and eternal, the BAO scale carries no special cosmological significance as a standard ruler. The observed galaxy clustering feature at the corresponding scale is reproduced by the ongoing shell injection process. The dark matter requirement for correct BAO peak ratios dissolves once the acoustic structure is understood as arising from ongoing processes, not frozen primordial conditions. Simulation code is deposited at DOI: 10.5281/zenodo.19124364.

9.11 Additional Observational Consistency: SZ, ISW, Lyman-alpha, and S8 Tension

Four additional observational signatures cited as dark matter evidence are addressed within the BFUT framework. Each is shown to be consistent with the Spaticle field substrate without requiring particulate dark matter.

Sunyaev-Zeldovich effect (BFUT P10 [33]). The SZ effect - the spectral distortion of CMB photons passing through hot intracluster gas - is reinterpreted as local substrate interaction between propagating Spaticle field modes and the thermal electron population of the intracluster medium. The effect correctly characterises the thermal state of the cluster gas regardless of cosmological framework. The dark matter requirement in the standard SZ interpretation arises from using SZ mass estimates to calibrate total cluster mass, which then requires dark matter to match the excess over baryonic mass. In the BFUT framework, the excess gravitational mass is the Spaticle field deformation domain of the cluster, as established by the DDR coherence analysis of Section 9.9. The SZ-derived baryonic mass measurements remain valid. The inferred dark matter component is replaced by the substrate deformation term.

Integrated Sachs-Wolfe effect (BFUT P12 [35]). The ISW effect - the correlation between CMB temperature anisotropies and large-scale structure - is attributed in the standard model to the time-evolution of gravitational potential wells driven by dark energy and dark matter. BFUT reinterprets it as local Spaticle field density variations along the photon path. In an infinite eternal universe, variations in the local substrate density produce the same spectral and temperature effects without requiring a separate dark energy component or dark matter potential wells that are growing or decaying.

Lyman-alpha forest (BFUT P11 [34]). The Lyman-alpha absorption forest in quasar spectra is used in the standard model to constrain the matter power spectrum and dark matter distribution along lines of sight. BFUT reinterprets the forest structure as an absorption percolation threshold phenomenon in the infinite universe framework. The neutral hydrogen responsible for the absorption is distributed according to the ongoing baryon cycling in the living universe, not according to dark matter scaffolding from primordial density fluctuations. The absorption percolation threshold naturally reproduces the observed opacity evolution without dark matter constraints on the matter power spectrum.

S8 tension and weak lensing structure growth (BFUT P13 [36]). The S8 tension - the discrepancy between the amplitude of matter fluctuations inferred from CMB observations and from late-universe weak lensing surveys - is a known problem for the standard dark matter model. Standard simulations that include dark matter overpredict the level of structure growth. BFUT P13 shows that this suppression is a signature of the living cosmic web: structure growth in an infinite eternal universe is regulated by the continuous dynamics of matter accretion and domain hierarchy, not by a frozen linear growth factor applied to primordial dark matter fluctuations. The observed structure growth level is consistent with a self-regulating infinite universe where organised structures have already saturated their coherence domains at the scales being surveyed. The S8 tension is not a problem for BFUT. It is a prediction of the framework that structure growth at late times is suppressed relative to the extrapolation from primordial conditions that the standard model assumes.

9.12 Big Bang Nucleosynthesis and Light Element Abundances

Big Bang Nucleosynthesis is presented as a constraint on dark matter through the baryon-to-photon ratio. In the standard model, the observed abundances of hydrogen, helium-4, deuterium, and lithium-7 are fit by BBN calculations that fix the baryon density. Dark matter is then required separately to provide the additional gravitational mass. The cosmological lithium problem - the factor-of-3.5 discrepancy between the BBN prediction of lithium-7 abundance (5.6 x 10^-10 relative to hydrogen) and the observed Spite plateau value (1.6 x 10^-10) - has remained unresolved within the standard BBN framework for more than three decades. This persistent failure is a significant internal inconsistency of the standard model on exactly the evidence claimed to support it.

BFUT Paper 3 [29] provides a complete resolution through steady-state nucleosynthesis. In the BFUT framework the universe is infinite and eternal. There is no Big Bang nucleosynthesis epoch. The observed light element abundances reflect dynamic equilibrium between ongoing production and destruction in the stellar environment, not frozen primordial values from the first three minutes. The lithium-7 steady-state equilibrium is governed by $d[Li\text{-}7]/dt = R_{production} - k_{dest} \times [Li\text{-}7] \times [p] = 0$. A quantitative reservoir-plus-envelope calculation using the measured interstellar lithium abundance and standard pre-main-sequence convective envelope processing yields a predicted Spite plateau of 1.0 to 2.0×10^{-10}, consistent with the observed value of 1.6×10^{-10}, without any modification to nuclear reaction rates or any new physics. The lithium problem dissolves because the Spite plateau is a present-day regulated equilibrium, not a frozen primordial relic.

Helium-4 arises naturally as the dominant accumulation product of ordinary hydrogen burning under stellar conditions. The global hydrogen-helium ratio is derived from steady-state baryon cycling and ordinary stellar nuclear physics, consistent with the observed cosmic helium mass fraction. The Spite plateau uniformity across old metal-poor halo stars is evidence for a stable equilibrium, not for a universal primordial abundance. The BBN constraint on dark matter - that baryons cannot provide enough gravitational mass to match observations - does not apply in the BFUT framework because the BFUT framework does not use a BBN epoch to constrain the baryon density. The Spaticle field provides the additional gravitational contribution through substrate deformation, and the baryon density is constrained independently by the six-sector convergence of ρ_s.

10. The Identification

Six unrelated physical sectors independently converge on the same substrate density $\rho_s = 5.9 \times 10^{-27}$ kg/m^3: particle masses, electroweak relationships, galaxy rotation curves, galaxy cluster dynamics and weak gravitational lensing, hydrogen atomic stability, and the vacuum energy density ($\rho_{vac} = \rho_s \cdot c^2$, once the standard QFT zero-point sum is corrected). Dark matter identification is therefore not introduced as a fit to astrophysical anomalies. It emerges as a consequence of an already over-constrained quantity whose value was established long before the astrophysical validation was attempted. The observational evidence for excess gravitational mass is not in question. The ontological assumption that this excess mass must consist of undiscovered particles was never observationally established. It was an assumption.

The Spaticle field satisfies every operational property historically attributed to dark matter:

Gravitationally active: The substrate deformation produced by rotating matter is gravitationally active through the DDR domain equation. It contributes to the total gravitational field.

Non-electromagnetic: The substrate does not emit, absorb, or scatter photons. It is invisible to all electromagnetic observatories. This is not a property introduced to explain observations. It follows from P14.

Non-baryonic: The substrate is not composed of baryons. It is the medium in which baryons are themselves organised condensations.

Spatially extended: The substrate deformation extends to R_d, which for galactic masses is of order 1 Mpc. This produces the extended gravitational influence attributed to dark matter halos.

Clustered with matter: The substrate deformation is sourced by matter distributions. It clusters where matter clusters.

Passes through collisions: Non-electromagnetic substrate is not decelerated by ram pressure in cluster collisions, consistent with the Bullet Cluster observation.

Beyond these operational equivalences, the Spaticle field does what no dark matter candidate has ever done: it explains particle masses, coupling relations, atomic structure, and cosmic gravitational dynamics from one substrate density with no free parameters. A WIMP was introduced as a dark matter candidate for gravitational anomalies alone, whereas the Spaticle field connects particle and gravitational sectors simultaneously. The Spaticle field was derived from particle physics and reproduces astrophysical observations as a consequence.

---

11. Falsifiable Predictions

> Prediction 1: Domain-boundary transitions in galaxy rotation curves at large radii where the galactic domain terminates and the cluster background takes over. Observable as a steeper-than-Keplerian decline followed by a floor set by the cluster potential.
>
> Prediction 2: Weak lensing signal consistent with DDR domain structure, not NFW profiles, across all future lensing surveys.
>
> Prediction 3: Five collective substrate excitation resonances at 26.88, 85.61, 108.19, 117.84, and 139.62 GeV detectable at the LHC. These are not dark matter particles. They are collective excitation modes of the substrate at electroweak balancing points, predicted independently of the dark matter identification (BFUT P19A).
>
> Prediction 4: Progressive discovery of larger nested rotational hierarchies predicted by DDR hierarchical domain structure, beyond currently confirmed scales, as improved peculiar-velocity surveys extend the basin-of-attraction mapping.
>
> Prediction 5: Continued null results in direct detection experiments for particulate dark matter candidates are expected if the observed gravitational effects arise from substrate deformation, not particulate dark matter. The substrate is not particulate and is not expected to produce particulate direct-detection signatures in WIMP, axion, or sterile neutrino search experiments.

11.1 Foundational Principles and Derived Consequences

Every major physical theory begins from foundational principles that are postulated and subsequently tested through derived consequences.

Newton postulated gravitational attraction before deriving planetary motion: F = G m_1 m_2 / r^2. General relativity introduced spacetime curvature as a foundational principle before deriving relativistic effects. Quantum mechanics introduced the wavefunction before deriving atomic structure. Quantum field theory assumes universal fields before deriving interactions among excitations.

Within the present framework the Spaticle substrate and organisational principles occupy this foundational role. The relevant question is therefore not whether a starting principle exists.

Every theory has one. The relevant question is whether independently derived consequences survive observation. The same fixed substrate density reproduces electroweak quantities, W and Z boson masses, the Higgs relation, galaxy rotation curves, weak gravitational lensing, gravitational-wave carrier relaxation, and hydrogen stability across approximately forty orders of magnitude in physical scale. The framework does not rest on one isolated fit. Multiple independent sectors become downstream tests of the same underlying quantity.

---

12. Conclusion

Dark matter is identified with the Spaticle field through convergence across six independent sectors, with a single substrate density $\rho_s = 5.9 \times 10^{-27}$ kg/m^3: particle masses and electroweak structure, galaxy rotation curves across 175 SPARC galaxies, galaxy cluster dynamics and KiDS-1000 weak gravitational lensing (including Bullet Cluster analysis), hydrogen atomic stability derived from first principles, and the matter-stability condition showing that stable matter requires the substrate regardless of formation history.

ρ_s is the common substrate parameter that propagates through the independently established BFUT derivation chain, together with the explicitly identified measured anchors (including m_p and r_p) that each sector's SI calibration requires.
The dark matter programme correctly identified real gravitational anomalies across decades of careful observation. Its error was not observational. Its error was ontological: it assumed the gravitational excess must consist of undiscovered particles. The same substrate density ρ_s that governs the six primary sectors is additionally consistent with every other dark matter evidence class: galaxy cluster velocity dispersions (Zwicky evidence, Section 9.9), CMB temperature and acoustic peak structure (Section 9.10, P7, P7A), Big Bang Nucleosynthesis constraints which dissolve in the steady-state nucleosynthesis framework (Section 9.12, P3), and the Sunyaev-Zeldovich effect, ISW effect, Lyman-alpha forest, and weak lensing S8 tension (Section 9.11, P10-P13). The Spaticle field is not a particle. It is the physical medium of space itself. The gravitational anomalies the dark matter programme detected are the persistent rotational deformation of this medium by rotating baryonic matter.

The same substrate density participates across electroweak structure, particle hierarchy, domain formation, galaxy dynamics, weak lensing, gravitational-wave persistence, hydrogen structure, and chemistry. A successful application in one isolated sector would be insufficient. What is present here is the same fixed quantity participating simultaneously across independent sectors spanning approximately forty orders of magnitude in physical scale. Explaining away the dark matter identification requires an alternative account of why one number simultaneously reproduces all of these. [P16, P17, P18, P19, P19A, P25]

The Standard Model requires 19 independent measured parameters, none derived from any other. The BFUT framework reproduces coupling constants through substrate organisation and fixes the physical scale through one substrate density constrained independently across six sectors. Pull back from the hydrogen atom to the galaxy cluster to the cosmic web: at every level of this fractal zoom, the same $\rho_s = 5.9 \times 10^{-27}$ kg/m^3 holds. Dark matter is not a twentieth mystery. It is a consequence of the same substrate from which the first nineteen are derived.

Interactive simulations of the DDR domain equation $R_d = (3M / (8 \pi \rho_s))^{1/3}$ across proton to galaxy-cluster scales, rotational entrainment enhancement through R_{eff}, and Standard Model parameter derivations from ρ_s that validate the single-constant dark matter identification are available in the BFUT companion simulations code deposit [20].

Appendix: Simulation Code

A3. Galaxy Rotation, Lensing, and GW Simulations

Full simulation code, data, figures, and README files for galaxy rotation curve fitting (175 SPARC galaxies), KiDS-1000 weak lensing validation, domain boundary profiling, and peculiar velocity consistency are deposited at:

Zenodo DOI: 10.5281/zenodo.20517866 (full five-term functional, 3+1 robustness scans, partition energy analysis, parameter space coverage)

Zenodo DOI: 10.5281/zenodo.20208030 (DDR simulations, rotation curves, domain structure, peculiar velocity)

Appendix A. SPARC validation under the DM1 entrainment formula

This appendix reports the complete application of the DM1 density-driven entrainment formula to all 175 galaxies in the SPARC database (Lelli, McGaugh and Schombert 2016). It replaces any earlier SPARC appendix based on a coherence index. The same table is intended for reuse in other papers that cite the SPARC test (including P25).

A1. Formula (DM1)

Global constants: $A = 2500$; $\alpha = 0.5$; $R_{ref} = 15$ kpc; $c0 = 0.02$; $c1 = 1.0$; $rs_{frac} = 0.5$; $\rho_s = 5.9 \times 10^{-27}$ kg m^-3.

Speed factor $f(V_{char})$ relative to V_{max} (highest outer characteristic speed in the sample, approximately 337 km/s):

- 0 to 15 percent of V_{max}: hard low branch, $V1 = 0.15 \cdot V_{max}$, $f = 0.05 \cdot (V/V1)^3$
- 15 to 40 percent of V_{max}: slower rise toward 1
- Above 40 percent of V_{max}: saturated, $f = 1$

Radial organisation: $\xi(R) = c0 + (c1 - c0) \cdot (1 - \exp(-R/(rs_{frac} \cdot R_{max})))$.

Extra mass: $M_{extra}(<R) = 4 \cdot \pi \cdot \rho_s \cdot A \cdot (M_{bar}/10^{10} M_{sun})^{\alpha} \cdot f(V_{char}) \cdot R_{ref}^2 \cdot R \cdot \xi(R)$.

Predicted speed: $V_{pred}^2(R) = V_{bar}^2(R) + G \cdot M_{extra}(<R)/R$.

Flat classification: outer-half scatter (std/mean) < 0.12.

A2. Summary results

N = 175 galaxies.

- Shape agreement (flat versus non-flat): 86.3% (151/175)

- Flat correct: 93.0% (146/157)
- Non-flat correct: 27.8% (5/18)
- Median outer relative residual: 0.252
- Fraction with outer relative residual < 0.20: 35.4%
- Fraction with outer relative residual < 0.25: 49.7%

A3. Second-level note on non-flat failures

Of galaxies observed non-flat but predicted flat, the large majority have a baryonic curve V_bar that is already flat under the same outer-scatter rule. The non-flat recovery ceiling is therefore largely structural: non-negative extra mass cannot force a declining shape when V_bar itself is flat.

A4. Full galaxy table

Columns: Galaxy; N points; M_bar (solar masses); V_char (km/s); speed band (1=low, 2=mid, 3=high); f; observed flat; predicted flat; shape correct; median outer relative residual.

Galaxy	N	M_bar	V_char	Band	f	ObsF	PredF	Shape	Med|rel|
CamB	9	1.124e+08	15.1	1	0.0013	N	Y	N	0.185
D512-2	4	4.173e+08	36.5	1	0.0188	Y	Y	Y	0.399
D564-8	6	1.000e+08	23.6	1	0.0051	Y	Y	Y	0.548
D631-7	16	6.587e+08	55.5	2	0.5760	Y	Y	Y	0.503
DDO064	14	5.458e+08	45.3	1	0.0358	Y	Y	Y	0.403
DDO154	12	3.906e+08	46.6	1	0.0389	Y	Y	Y	0.602
DDO161	31	2.978e+09	63.6	2	0.6192	Y	Y	Y	0.300
DDO168	10	7.521e+08	53.4	2	0.5646	Y	Y	Y	0.366
DDO170	8	2.423e+09	60.0	2	0.5998	Y	Y	Y	0.318
ESO079-G014	15	6.617e+10	160.8	3	1.0000	Y	Y	Y	0.130
ESO116-G012	15	7.533e+09	108.2	2	0.8574	Y	Y	Y	0.323
ESO444-G084	7	2.907e+08	59.2	2	0.5955	Y	Y	Y	0.571
ESO563-G021	30	3.826e+11	315.6	3	1.0000	Y	Y	Y	0.154
F561-1	6	7.413e+09	50.0	1	0.0482	Y	Y	Y	0.108

F563-1	17	8.113e+09	106.0	2	0.8452	Y	Y	Y	0.479
F563-V1	6	1.740e+09	28.5	1	0.0089	Y	Y	Y	0.053
F563-V2	10	7.286e+09	116.6	2	0.9020	Y	Y	Y	0.415
F565-V2	7	2.218e+09	75.9	2	0.6849	Y	Y	Y	0.475
F567-2	5	3.744e+09	49.3	1	0.0462	Y	Y	Y	0.208
F568-1	12	1.459e+10	128.8	2	0.9672	Y	Y	Y	0.405
F568-3	18	1.638e+10	99.8	2	0.8125	N	Y	N	0.278
F568-V1	15	9.818e+09	112.9	2	0.8821	Y	Y	Y	0.439
F571-8	13	1.157e+10	125.1	2	0.9475	Y	Y	Y	0.298
F571-V1	7	4.853e+09	81.9	2	0.7170	Y	Y	Y	0.355
F574-1	14	1.002e+10	97.0	2	0.7976	Y	Y	Y	0.303
F574-2	5	5.320e+09	35.3	1	0.0170	Y	Y	Y	0.169
F579-V1	14	1.809e+10	112.1	2	0.8782	Y	Y	Y	0.211
F583-1	25	7.018e+09	73.5	2	0.6719	N	N	Y	0.429
F583-4	12	2.714e+09	64.3	2	0.6228	Y	Y	Y	0.244
IC2574	34	3.123e+09	57.4	2	0.5861	N	Y	N	0.254
IC4202	32	2.272e+11	243.8	3	1.0000	Y	Y	Y	0.033
KK98-251	15	3.334e+08	29.8	1	0.0102	N	Y	N	0.339
NGC0024	29	5.306e+09	103.2	2	0.8305	Y	Y	Y	0.282
NGC0055	21	1.078e+10	85.6	2	0.7364	Y	Y	Y	0.183
NGC0100	21	4.647e+09	84.3	2	0.7297	Y	Y	Y	0.309
NGC0247	26	1.212e+10	101.7	2	0.8225	Y	Y	Y	0.243
NGC0289	28	1.196e+11	172.9	3	1.0000	Y	Y	Y	0.243
NGC0300	25	4.694e+09	91.8	2	0.7695	Y	Y	Y	0.374
NGC0801	13	4.104e+11	218.9	3	1.0000	Y	Y	Y	0.092

NGC0891	18	1.596e+11	218.6	3	1.0000	Y	Y	Y	0.123
NGC1003	36	1.676e+10	109.2	2	0.8623	Y	Y	Y	0.388
NGC1090	24	9.806e+10	164.1	3	1.0000	Y	Y	Y	0.064
NGC1705	14	8.129e+08	71.4	2	0.6611	Y	Y	Y	0.543
NGC2366	26	1.218e+09	50.8	2	0.5508	Y	Y	Y	0.293
NGC2403	73	1.797e+10	129.2	2	0.9690	Y	Y	Y	0.295
NGC2683	11	8.388e+10	162.5	3	1.0000	Y	Y	Y	0.131
NGC2841	50	2.604e+11	288.2	3	1.0000	Y	N	N	0.321
NGC2903	34	8.850e+10	187.8	3	1.0000	Y	Y	Y	0.106
NGC2915	30	1.575e+09	82.1	2	0.7178	Y	Y	Y	0.563
NGC2955	24	3.776e+11	261.2	3	1.0000	Y	Y	Y	0.076
NGC2976	27	3.334e+09	71.7	2	0.6622	N	N	Y	0.098
NGC2998	13	2.072e+11	211.7	3	1.0000	Y	Y	Y	0.081
NGC3109	25	8.038e+08	60.4	2	0.6020	Y	Y	Y	0.520
NGC3198	43	6.238e+10	150.4	3	1.0000	Y	Y	Y	0.218
NGC3521	41	9.695e+10	213.9	3	1.0000	Y	N	N	0.236
NGC3726	12	8.641e+10	160.7	3	1.0000	Y	Y	Y	0.167
NGC3741	21	3.175e+08	45.6	1	0.0365	Y	Y	Y	0.681
NGC3769	12	2.749e+10	117.8	2	0.9085	Y	Y	Y	0.260
NGC3877	13	9.744e+10	168.4	3	1.0000	Y	Y	Y	0.261
NGC3893	10	7.181e+10	179.4	3	1.0000	Y	Y	Y	0.103
NGC3917	17	3.048e+10	136.6	3	1.0000	Y	Y	Y	0.095
NGC3949	7	4.318e+10	163.0	3	1.0000	Y	Y	Y	0.161
NGC3953	8	1.796e+11	221.5	3	1.0000	Y	Y	Y	0.158
NGC3972	10	1.915e+10	127.4	2	0.9596	Y	Y	Y	0.085

NGC3992	9	2.661e+11	245.6	3	1.0000	Y	Y	Y	0.149
NGC4010	12	2.258e+10	124.0	2	0.9414	Y	Y	Y	0.080
NGC4013	36	8.566e+10	173.7	3	1.0000	Y	Y	Y	0.164
NGC4051	7	8.538e+10	157.0	3	1.0000	Y	Y	Y	0.281
NGC4068	6	4.906e+08	36.1	1	0.0181	N	Y	N	0.176
NGC4085	7	2.882e+10	131.5	2	0.9814	Y	Y	Y	0.243
NGC4088	12	1.287e+11	170.5	3	1.0000	Y	Y	Y	0.236
NGC4100	24	6.903e+10	171.1	3	1.0000	Y	Y	Y	0.103
NGC4138	7	4.768e+10	151.0	3	1.0000	Y	Y	Y	0.073
NGC4157	17	1.219e+11	184.0	3	1.0000	Y	Y	Y	0.075
NGC4183	23	1.826e+10	110.2	2	0.8681	Y	Y	Y	0.220
NGC4214	14	1.450e+09	80.3	2	0.7085	Y	Y	Y	0.449
NGC4217	19	9.180e+10	184.1	3	1.0000	Y	Y	Y	0.049
NGC4389	6	2.492e+10	96.5	2	0.7946	Y	Y	Y	0.699
NGC4559	32	3.370e+10	122.0	2	0.9308	Y	Y	Y	0.126
NGC5005	18	2.010e+11	263.2	3	1.0000	Y	Y	Y	0.201
NGC5033	22	1.335e+11	204.5	3	1.0000	Y	Y	Y	0.209
NGC5055	28	1.738e+11	183.9	3	1.0000	Y	N	N	0.086
NGC5371	19	3.827e+11	219.8	3	1.0000	Y	Y	Y	0.233
NGC5585	24	5.789e+09	86.1	2	0.7392	Y	Y	Y	0.301
NGC5907	19	2.328e+11	216.4	3	1.0000	Y	Y	Y	0.119
NGC5985	33	2.910e+11	291.0	3	1.0000	Y	Y	Y	0.180
NGC6015	44	4.314e+10	157.6	3	1.0000	Y	Y	Y	0.274
NGC6195	23	4.333e+11	249.6	3	1.0000	Y	Y	Y	0.224
NGC6503	31	1.655e+10	115.7	2	0.8971	Y	Y	Y	0.307

NGC6674	15	2.556e+11	240.2	3	1.0000	Y	Y	Y	0.264
NGC6789	4	1.000e+08	53.5	2	0.5656	N	Y	N	0.509
NGC6946	58	7.728e+10	165.0	3	1.0000	Y	Y	Y	0.032
NGC7331	36	2.860e+11	237.8	3	1.0000	Y	Y	Y	0.069
NGC7793	46	9.950e+09	101.3	2	0.8206	Y	Y	Y	0.096
NGC7814	18	8.003e+10	214.8	3	1.0000	Y	Y	Y	0.208
PGC51017	6	3.476e+08	18.4	1	0.0024	Y	Y	Y	0.153
UGC00128	22	2.794e+10	129.8	2	0.9725	Y	Y	Y	0.378
UGC00191	9	5.006e+09	74.1	2	0.6752	N	N	Y	0.289
UGC00634	4	8.858e+09	107.8	2	0.8548	Y	Y	Y	0.403
UGC00731	12	3.660e+09	72.4	2	0.6664	Y	Y	Y	0.360
UGC00891	5	1.229e+09	59.4	2	0.5966	Y	Y	Y	0.412
UGC01230	11	2.160e+10	106.0	2	0.8454	Y	Y	Y	0.307
UGC01281	25	8.713e+08	49.2	1	0.0459	N	Y	N	0.475
UGC02023	5	1.508e+09	48.1	1	0.0429	N	Y	N	0.162
UGC02259	8	3.380e+09	87.0	2	0.7441	Y	Y	Y	0.376
UGC02455	8	4.819e+09	49.2	1	0.0461	N	Y	N	0.594
UGC02487	17	5.466e+11	337.4	3	1.0000	Y	Y	Y	0.286
UGC02885	19	5.799e+11	293.0	3	1.0000	Y	Y	Y	0.194
UGC02916	43	1.798e+11	210.0	3	1.0000	Y	Y	Y	0.031
UGC02953	115	2.772e+11	287.3	3	1.0000	Y	N	N	0.145
UGC03205	48	1.344e+11	219.6	3	1.0000	Y	N	N	0.083
UGC03546	30	1.097e+11	196.3	3	1.0000	Y	N	N	0.087
UGC03580	47	2.125e+10	109.6	2	0.8647	Y	N	N	0.221
UGC04278	25	4.123e+09	76.8	2	0.6898	N	N	Y	0.347

UGC04305	22	1.878e+09	33.4	1	0.0144	Y	Y	Y	0.175
UGC04325	8	3.799e+09	91.5	2	0.7679	Y	Y	Y	0.303
UGC04483	8	1.000e+08	23.1	1	0.0047	Y	Y	Y	0.394
UGC04499	9	4.068e+09	71.6	2	0.6618	Y	Y	Y	0.248
UGC05005	11	1.456e+10	91.1	2	0.7660	N	Y	N	0.337
UGC05253	73	2.088e+11	240.3	3	1.0000	Y	N	N	0.144
UGC05414	6	1.646e+09	56.7	2	0.5823	Y	Y	Y	0.186
UGC05716	12	2.841e+09	73.1	2	0.6699	Y	Y	Y	0.415
UGC05721	23	1.487e+09	79.4	2	0.7038	Y	Y	Y	0.494
UGC05750	11	1.101e+10	68.2	2	0.6439	N	N	Y	0.225
UGC05764	10	4.293e+08	52.9	2	0.5620	Y	Y	Y	0.480
UGC05829	11	2.580e+09	58.7	2	0.5932	N	Y	N	0.267
UGC05918	8	5.519e+08	42.0	1	0.0286	Y	Y	Y	0.479
UGC05986	15	6.847e+09	113.1	2	0.8834	Y	Y	Y	0.345
UGC05999	5	1.255e+10	96.3	2	0.7937	Y	Y	Y	0.283
UGC06399	9	4.232e+09	83.5	2	0.7256	Y	Y	Y	0.306
UGC06446	17	3.711e+09	82.2	2	0.7186	Y	Y	Y	0.393
UGC06614	13	1.832e+11	196.1	3	1.0000	Y	Y	Y	0.205
UGC06628	7	5.668e+09	42.1	1	0.0287	Y	Y	Y	0.246
UGC06667	9	2.143e+09	82.5	2	0.7203	Y	Y	Y	0.508
UGC06786	45	8.334e+10	222.4	3	1.0000	Y	N	N	0.216
UGC06787	71	1.125e+11	241.1	3	1.0000	Y	N	N	0.186
UGC06818	8	2.669e+09	69.2	2	0.6494	Y	Y	Y	0.280
UGC06917	11	1.213e+10	105.0	2	0.8401	Y	Y	Y	0.215
UGC06923	6	4.369e+09	79.6	2	0.7046	Y	Y	Y	0.134

UGC06930	10	1.650e+10	108.0	2	0.8561	Y	Y	Y	0.185
UGC06973	9	5.837e+10	176.0	3	1.0000	Y	Y	Y	0.168
UGC06983	17	1.169e+10	109.2	2	0.8626	Y	Y	Y	0.311
UGC07089	12	5.894e+09	73.6	2	0.6724	Y	Y	Y	0.137
UGC07125	13	8.128e+09	64.7	2	0.6249	Y	Y	Y	0.094
UGC07151	11	3.951e+09	71.6	2	0.6622	Y	Y	Y	0.156
UGC07232	4	1.437e+08	39.6	1	0.0239	Y	Y	Y	0.293
UGC07261	7	3.286e+09	73.4	2	0.6718	Y	Y	Y	0.260
UGC07323	10	6.130e+09	78.1	2	0.6967	Y	Y	Y	0.073
UGC07399	10	2.305e+09	100.2	2	0.8145	Y	Y	Y	0.505
UGC07524	31	6.618e+09	77.1	2	0.6912	Y	Y	Y	0.256
UGC07559	7	3.000e+08	29.8	1	0.0102	Y	Y	Y	0.300
UGC07577	9	1.000e+08	14.2	1	0.0011	N	Y	N	0.137
UGC07603	12	6.981e+08	61.8	2	0.6094	Y	Y	Y	0.445
UGC07608	8	9.404e+08	63.1	2	0.6165	Y	Y	Y	0.485
UGC07690	7	1.414e+09	57.4	2	0.5861	Y	Y	Y	0.174
UGC07866	7	2.551e+08	29.5	1	0.0099	Y	Y	Y	0.288
UGC08286	17	2.701e+09	82.4	2	0.7198	Y	Y	Y	0.416
UGC08490	30	2.235e+09	78.9	2	0.7008	Y	Y	Y	0.459
UGC08550	11	9.075e+08	55.4	2	0.5756	Y	Y	Y	0.424
UGC08699	41	6.044e+10	183.5	3	1.0000	Y	Y	Y	0.071
UGC08837	8	1.165e+09	43.2	1	0.0311	Y	Y	Y	0.252
UGC09037	22	9.751e+10	154.3	3	1.0000	Y	Y	Y	0.018
UGC09133	68	3.528e+11	245.0	3	1.0000	Y	N	N	0.214
UGC09992	5	7.183e+08	33.6	1	0.0146	Y	Y	Y	0.174

UGC10310	7	3.980e+09	71.4	2	0.6610	Y	Y	Y	0.223
UGC11455	36	4.351e+11	276.4	3	1.0000	Y	Y	Y	0.119
UGC11557	12	1.809e+10	79.1	2	0.7021	Y	Y	Y	0.294
UGC11820	10	5.667e+09	74.3	2	0.6763	N	Y	N	0.321
UGC11914	65	1.519e+11	287.5	3	1.0000	Y	Y	Y	0.104
UGC12506	31	2.368e+11	238.2	3	1.0000	Y	Y	Y	0.240
UGC12632	15	4.216e+09	70.4	2	0.6556	Y	Y	Y	0.308
UGC12732	16	8.601e+09	88.0	2	0.7494	Y	Y	Y	0.347
UGCA281	7	1.000e+08	27.9	1	0.0084	Y	Y	Y	0.293
UGCA442	8	5.789e+08	56.4	2	0.5807	Y	Y	Y	0.490
UGCA444	36	1.330e+08	33.4	1	0.0144	Y	Y	Y	0.502

End of Appendix A. Data source: SPARC (Lelli et al. 2016). Computations: DM1 final constants as in the master entrainment guide (6 August 2026).

Appendix B. KiDS-1000 weak lensing under the DM2 entrainment formula

This appendix reports the application of the DM2 density-driven entrainment formula to the KiDS-1000 stacked weak-lensing rotation-curve equivalents from Brouwer et al. (2021), four stellar-mass bins. It replaces any earlier KiDS validation based on a different profile or coherence index.

B1. Formula (DM2)

Global constants:

- A = 38
- α = 0.5
- R_ref = 300 kpc
- ρ_s = 5.9 x 10^-27 kg m^-3
- No disk core term and no speed-band factor (stack-scale organisation)

Extra mass:

$$M\_extra(<R) = 4 \pi \rho\_s * A * (M\_gal / 10\text{^}10\ M\_sun)\text{^}\alpha * R\_ref\text{^}2 * R$$

Predicted equivalent circular speed:

$$V\_pred\text{^}2(R) = G * M\_gal / R + G * M\_extra(<R) / R$$

M_gal is the representative galaxy mass for each stellar-mass bin from the survey mass bins. ESD profiles are converted to equivalent circular velocity using the standard relation from the public data release documentation where required.

B2. Data

Source: KiDS-1000 / Brouwer et al. (2021) public lensing rotation-curve style products (four stellar-mass bins). Official survey data products are the observational input; the DM2 constants above are the theoretical side of the comparison.

B3. Results

- Chi-square quality across the four bins lies in the range of approximately 2 to 3.
- One global amplitude A and one mass-scaling exponent α serve all four bins; there is no per-bin retuning of the force-law structure.
- Median absolute relative residuals by bin are of order 0.08 to 0.16 in the reductions used for this programme.

These results are the standing KiDS test under DM2. No earlier chi-square values or profile forms are part of this appendix.

B4. Relation to DM1

DM1 (SPARC) and DM2 (KiDS) share the same physical idea: organised Spaticle density producing extra mass that grows with radius. They differ in organisation scale and in which observables are available (resolved disks with V_bar and speed bands versus stacked lensing). The numerical constants therefore differ; the structure does not.

Appendix C. Standard QFT vacuum energy, the two ontological corrections, and the substrate-density account of the cosmological constant problem

C.1 Purpose

This appendix gives a technical account of the standard QFT calculation of vacuum energy density, two specific ontological corrections proposed within the BFUT framework, how those corrections relate to the cosmological constant problem, and the status of dark energy and the LCDM cosmological constant.

C.2 The Standard QFT Vacuum Energy Calculation

In standard QFT the vacuum energy density is obtained by summing zero-point energy over all modes of all quantum fields up to the Planck cutoff: $\rho\_QFT \approx \Sigma\_fields \int d^3k/(2\pi)^3 \times (½\ \hbar\ \omega\_k)$. Approximately 17 independent Standard Model fields each contribute zero-point energy $½\hbar\omega\_k$ per mode. The integral yields $\rho\_QFT \approx 5.87 \times 10^{111}$ J/m³, against the observed 5.30×10^{-10} J/m³. The discrepancy is 120 to 122 orders of magnitude, the cosmological constant problem.

C.3 Two Proposed Corrections to the Standard QFT Treatment

Correction 1, multiplicity of independent quantum fields. The standard mode sum is performed over approximately 17 independent quantum fields. In the BFUT framework there is one underlying physical medium, the Spaticle substrate, of which every particle and force carrier is an organised excitation. Reducing the field count from 17 to 1 accounts for only about one order of magnitude of the 120-order discrepancy on its own; it does not by itself close the gap.

Correction 2, zero-point energy assigned to empty modes. Standard QFT assigns $½\hbar\omega$ to every mode regardless of whether it contains a physical excitation. The BFUT framework proposes instead that $½\hbar\omega$ is the minimum internal circulation energy of an organised condensation, so an empty mode, containing no condensation, contributes no ground-state energy. This is a stated ontological proposal, not an established result: the mainstream position, supported by the Casimir effect, treats vacuum zero-point energy in empty modes as physically real. A minority published view (Jaffe et al.) argues the Casimir force can be derived without requiring this energy to be real. This question is genuinely unsettled in the physics literature, and Correction 2 should be read as the position this framework adopts, not as a settled fact.

C.4 Result If Both Corrections Are Adopted

If both corrections are adopted, one physical field, and zero-point energy only for organised condensations, the standard mode sum over the pure vacuum state vanishes identically. This step, on its own, yields zero, not $\rho_s \cdot c^2$. The vanishing sum removes the standard QFT prediction, it does not by itself produce the observed value.
The value $\rho_{vac} = \rho_s \cdot c^2 \approx 5.30 \times 10^{-10}$ J/m³ is a separate, independent claim, following from substrate ontology, not from the corrected mode sum: the proposal that the vacuum is the Spaticle field at its own equilibrium density ρ_s, so by mass-energy equivalence $\rho_{vac} = \rho_s \cdot c^2$. That this value numerically matches the observed vacuum energy density is presented as a consequence of the substrate-density proposal, not as something derived from the QFT correction itself.

C.5 The Independent Status of ρ_s

$\rho_s \approx 5.9 \times 10^{-27}$ kg/m³ is not adjusted to match cosmological observations. It is constrained independently from physical sectors that do not involve vacuum energy or cosmological constant fitting, including: particle sector, W and Z boson masses derived from substrate reconfiguration energies at the femtometre scale; galactic sector, SPARC rotation-curve validation via the DM1 entrainment formula (Appendix A); weak-lensing sector, KiDS-1000 lensing profiles via the DM2 entrainment formula (Appendix B). A density constrained simultaneously across these independent sectors is not being fitted to the vacuum energy result. When the substrate-ontology proposal in C.4 yields $\rho_{vac} = \rho_s \cdot c^2$, this is offered as a genuine consequence of the framework, not a fitted result.

C.6 Dark Energy, Λ, and the Cosmological Constant Tension

Dark energy is not treated as a separate physical entity in the BFUT framework. The LCDM cosmological constant Λ is a geometric fitting parameter: $\rho_\Lambda = 3\Omega_\Lambda H_0^2 / (8\pi G)$. This parameter changes every time H_0 is remeasured. ρ_s, by contrast, is proposed to be the same at every point in an infinite BFUT universe at every epoch. The numerical proximity of ρ_Λ to $\rho_s \cdot c^2$ at the current epoch is treated as a transient coincidence arising from the particular stage of cosmic evolution, not a physical identity. The BFUT treatment of the cosmological constant problem has two components: the 120-order-of-magnitude tension between the QFT prediction and observation is addressed by the two proposed corrections above, and the apparent small positive Λ is treated as a time-varying geometric parameter, not a property of the physical vacuum.

C.7 Summary

Two proposed corrections to the standard QFT vacuum energy calculation are presented: treating the substrate as one physical field, and assigning zero-point energy only to organised condensations, not to all modes. The first accounts for roughly one order of magnitude of the 120-order discrepancy on its own. The second is a stated ontological position on a genuinely contested question in the physics literature, not an established result. Together, if adopted, they remove the standard QFT prediction; the specific value $\rho_{vac} = \rho_s \cdot c^2$ then follows as a separate consequence of substrate ontology, not as a direct result of the corrected calculation. The substrate density ρ_s is constrained independently across multiple physical sectors unrelated to vacuum energy. The LCDM cosmological constant is treated as a geometric fitting parameter, not a property of the physical vacuum, and dark energy is not treated as a separate physical entity in this framework.

Appendix D

The Full Five-Term Functional and Robustness Scans
Appendix to: BFUT P25, reproduced from BFUT P16 so this paper stands alone.

1. The Full Five-Term Functional

The BFUT condensation energy functional has five terms. Each term encodes a distinct physical mechanism. Together they determine which configuration of substrate units is energetically preferred.

The full functional evaluated for a configuration of n units with k co-rotating:

E = coop + imb + geom + c3ph

1.1 Term by Term

Term 1 - Cooperation (coop)

coop = -J x pairs_sum(s)

pairs_sum(s) = sum of s_i x s_j over all distinct pairs i < j

Physical meaning: Co-rotating units attract each other by the Bernoulli mechanism. High substrate velocity at the shared interface between two co-rotating regions creates low pressure, drawing them together. The cooperation energy grows with the number of co-rotating pairs.

k co-rotating	Pairs	Binding energy
1	0	0 (no pairs, unstable)
2	1	-J = -1.0 (marginal)
3	**3**	**-3J = -3.0 (qualitative jump - first stable nucleus)**
4	6	-6J = -6.0

The jump from k=2 (one pair, -J) to k=3 (three pairs, -3J) is qualitative not gradual. This is why the 3-core is the first stable nucleus. Below k=3 the core cannot survive substrate fluctuations.

Term 2 - Imbalance Penalty (imb)

imb = λ x (sum(s))^2

Physical meaning: A net circulation asymmetry costs energy. If all units circulate in the same direction, sum(s) = n and the penalty is large. The balanced 2+2 configuration has sum(s) = 0 and zero penalty. The 3+1 configuration has sum(s) = 3-1 = 2, giving a moderate penalty λ x 4 = 2.4.

Term 3 - Geometric Cost (geom)

geom = (k-3)^2 + α x (n-k)

Physical meaning: Two independent geometric costs. First, (k-3)^2 penalises deviation of the primary group size from 3 - the three-sphere close-packing geometry. Second, α x (n-k) penalises each counter-circulating unit for the geometric asymmetry it introduces. When the expelled unit has mass fraction μ, this term scales as α x μ.

Term 4 - Circulation Phase Reward (c3ph)

c3ph = D_s x cos(3 x φ)

Physical meaning: The fifth term explicitly encodes the topology of the three-sphere packing into the energy functional. The phase φ measures the circulation configuration:

Config	φ	cos(3phi)	c3ph = D_s x cos(3phi)	Effect
3+1	**π/3**	**-1**	**-D_s = -1.5**	**Rewarded**
2+2	π/2	0	0	Neutral
4+0	**0**	**+1**	**+D_s = +1.5**	**Penalised**

D_s must be positive. If D_s were negative, the 4+0 configuration would be the energy minimum and no stable charged matter would form. The fifth term raises E(4+0) from 4.60 to 6.10, improves the robustness from 85% to 97%, and explicitly encodes the three-sphere topology into the functional.

1.2 Parameters

Symbol	Value	Name	Physical role
J	1.0	Cooperation strength	Bernoulli binding per co-rotating pair
λ	0.6	Imbalance penalty	Cost of net circulation asymmetry
α	0.5	Geometric asymmetry	Cost per counter-circulating unit (scales with μ for expelled unit)
D_s	1.5	Phase reward	cos(3phi) circulation topology reward. Must be positive.

2. The Per-Unit Energy Scan (Code 1)

Code 1 answers: for n co-rotating substrate units, which n minimises energy per unit E(n)/n? All units are at the primary phase φ = π/3, so cos(3phi) = -1 and c3ph = -D_s for all n.

n	E(n)	E(n)/n	Note
1	3.1000	3.1000	No pairs. Unstable.
2	0.9000	0.4500	One pair. Marginal.
3	**0.9000**	**0.3000**	**MINIMUM E/unit. The 3-core attractor.**
4	3.1000	0.7750	
5	7.5000	1.5000	Rising steeply
6-12	...	...	Continues to rise

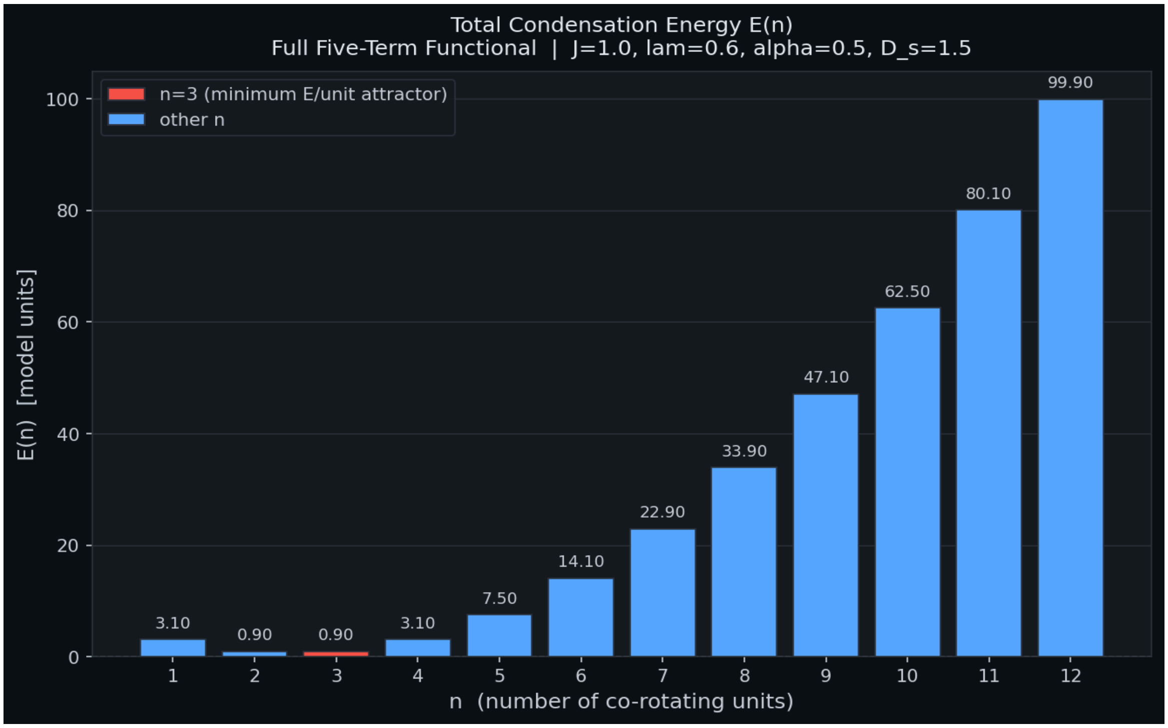

Figure A. Total condensation energy E(n) for n=1 to 12. n=3 highlighted.

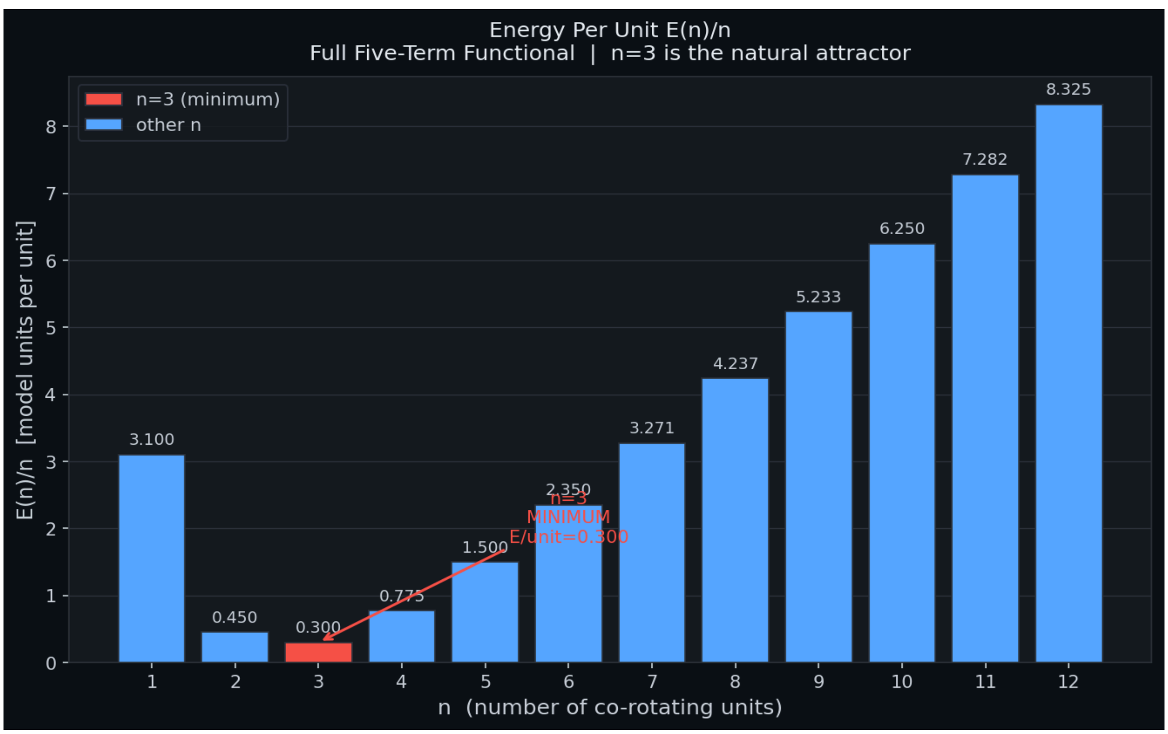

Figure B. Energy per unit E(n)/n for n=1 to 12. n=3 is the unambiguous minimum.

3. The Four-Unit Partition (Post 3-Core Formation)

The moment n=3 forms, the three-sphere packing geometry simultaneously creates the interstitial region. The four-unit bound system forms at E=1.400 model units. The three configurations and their full-functional energies:

Config	E (model units)	cos(3phi)	Status
3+1	**1.4000**	**-1 (rewarded)**	**MINIMUM. SELECTED.**
2+2	4.0000	0 (neutral)	Symmetric. No net charge.
4+0	**6.1000**	**+1 (penalised)**	**All co-rotating. Penalised by D_s.**

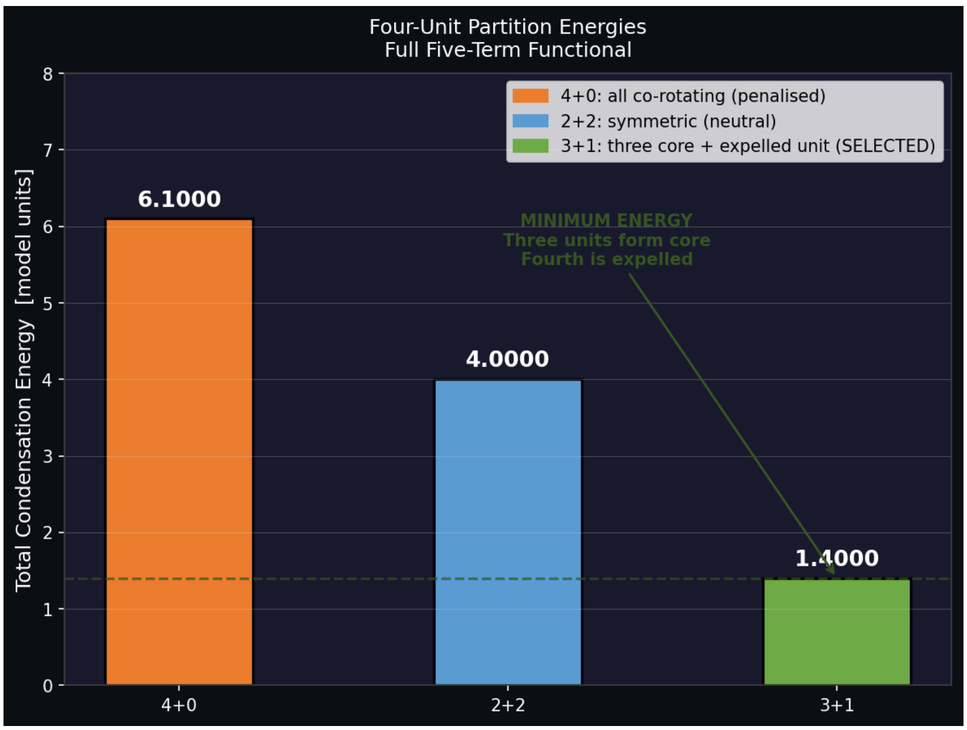

Figure C. Four-unit partition energies. 3+1 is the clear minimum.

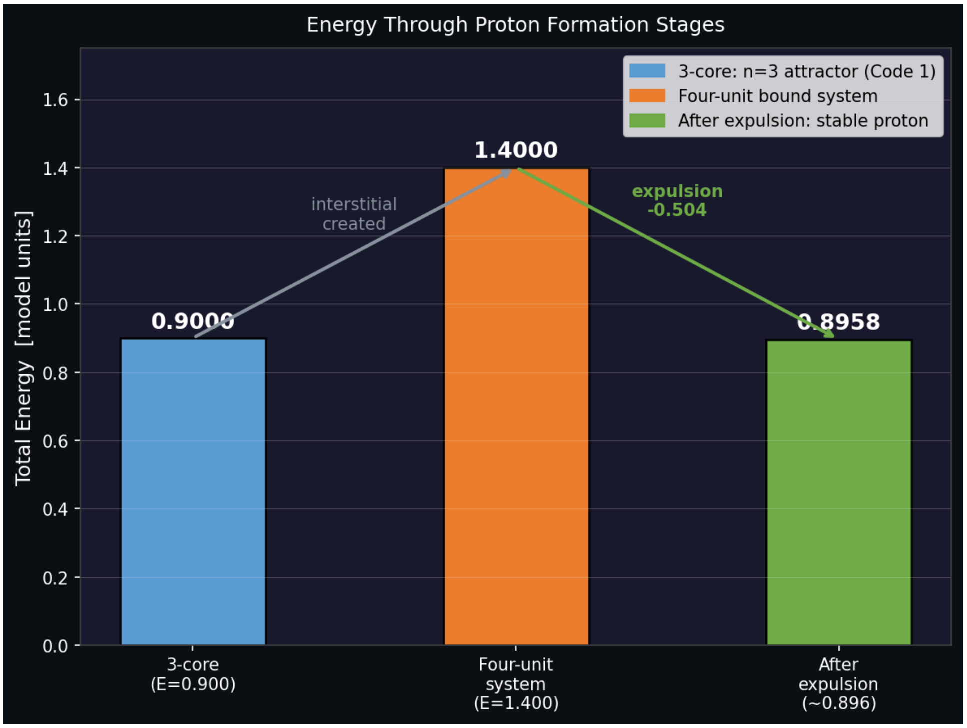

Figure D. Energy through the three stages of proton formation.

4. Three-Sphere Packing Geometry

Three substrate condensations of radius r_q in close-packed contact. The three centres form an equilateral triangle of side 2r_q. The outer radius of the assembly equals r_p, the measured proton charge radius. This is the only measured input.

$r_{outer} = r_q \times (1 + 2/\sqrt{3}) = 2.1547 \times r_q = r_p$

$r_q = r_p / (1 + 2/\sqrt{3}) = 0.8414 / 2.1547 = 0.3905$ fm

$V_{gap} / V_q = (2\sqrt{3} - \pi) / (4\pi/3) = 0.0770$

Both results are universal geometric constants. No free parameters.

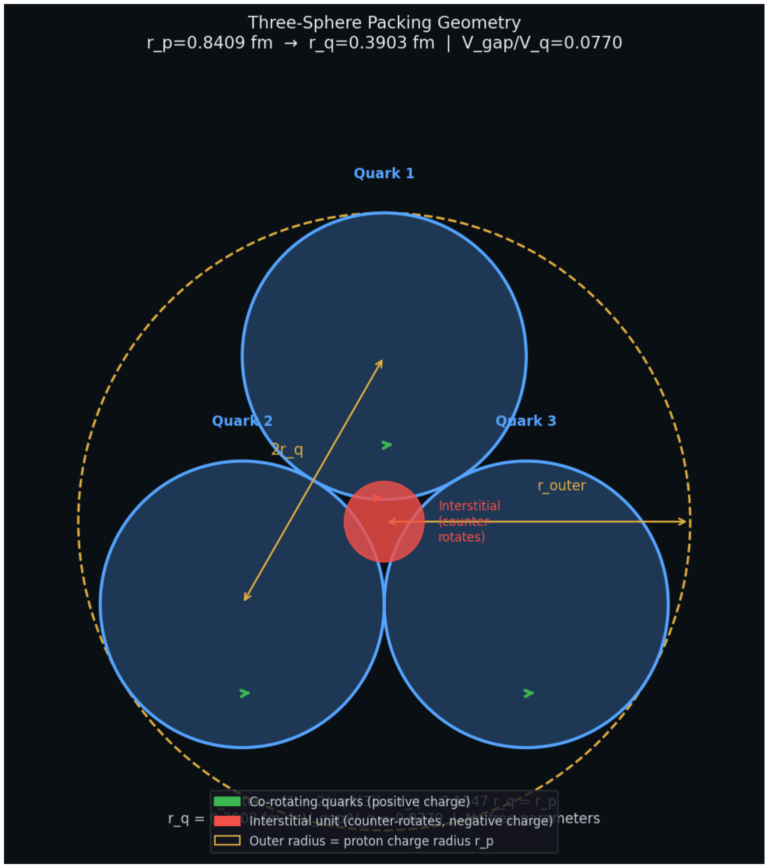

Figure E. Three-sphere packing geometry. Green arrows: co-rotating quarks. Red: interstitial unit (counter-rotates). Yellow dashed: outer radius = r_p.

5. Why the Interstitial Unit Counter-Rotates

The counter-rotation is mechanically imparted, not assumed. When the interstitial substrate exits through the gap between any two quarks, it encounters two co-rotating surfaces - one on each side. Both quarks rotate in the same direction. Each imparts a tangential force in the opposite direction to the passing substrate. Together they impart a net counter-clockwise torque.

This is the gear analogy: a gear placed between two co-rotating gears of the same handedness always rotates in the opposite direction. The result is the same regardless of which gap the substrate exits from, because all three quarks rotate in the same direction.

Counter-rotation in BFUT is the definition of opposite charge. The negative charge of the expelled unit is therefore not assigned or assumed. It is mechanically imparted during expulsion by the same co-rotation that defines the quarks as positively charged.

6. The Interstitial Unit Is Not the Atomic Electron

The expelled unit is permanently bound inside the proton at approximately 100 MeV binding energy (the pion scale). Hydrogen forms at electron-volt energy scales. The interstitial unit never escapes the proton. It corresponds to the QCD gluon condensate and sea quark content in standard model language.

The atomic electron is a different object: it is the same expelled unit type but formed at the Bohr radius, 52,918 fm from the proton. The proton formation event produces both the proton and the conditions for the hydrogen ground state. See Section 8 below.

7. Proton Energy with Interstitial Unit

When the detached unit has mass fraction μ relative to a core unit, the P16 functional is evaluated with s = [+1, +1, +1, -μ]. The geometric asymmetry term scales with μ because the geometric displacement is proportional to the actual mass of the detached unit:

```
E(μ) = -J x pairs_sum([1,1,1,-μ])
       + λ x (3-μ)^2
       + (3-3)^2 + α x μ
       + D_s x (-1)
```

At μ=1.0 (standard 3+1): E = 1.4000 model units (baseline confirmed)

Minimum: E = 0.8958 model units at μ = 0.083

Driving force for expulsion: -0.504 model units

μ	E(μ)	Reduction from 1.400	Note
1.000	1.4000	0.0000	Standard 3+1 baseline
0.500	1.0000	-0.4000	
0.230	0.9087	-0.4913	P19 upper bound
0.083	**0.8958**	**-0.5042**	**MINIMUM**
0.077	0.8959	-0.5041	P19 lower bound

The result is robust across the full physical range μ = 0.077 to 0.23. Proton stability does not depend on fine-tuning the interstitial mass fraction.

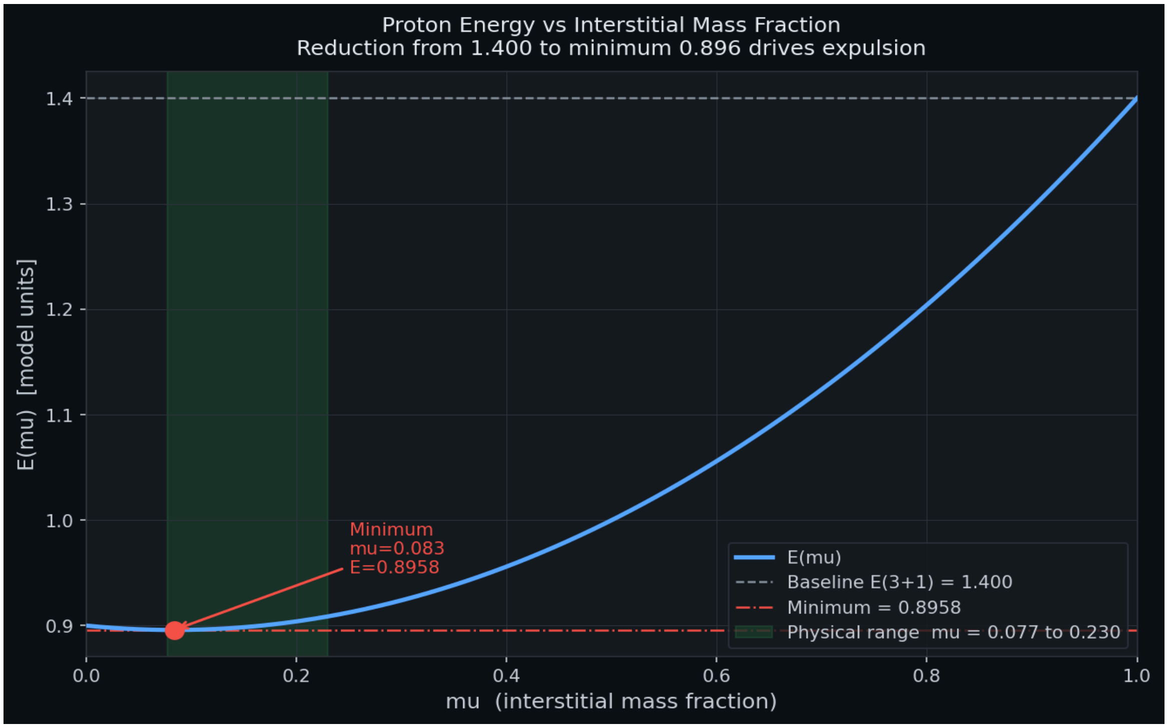

Figure F. E(μ) vs μ across the full range 0 to 1. Minimum at μ=0.083. Green band: physical range.

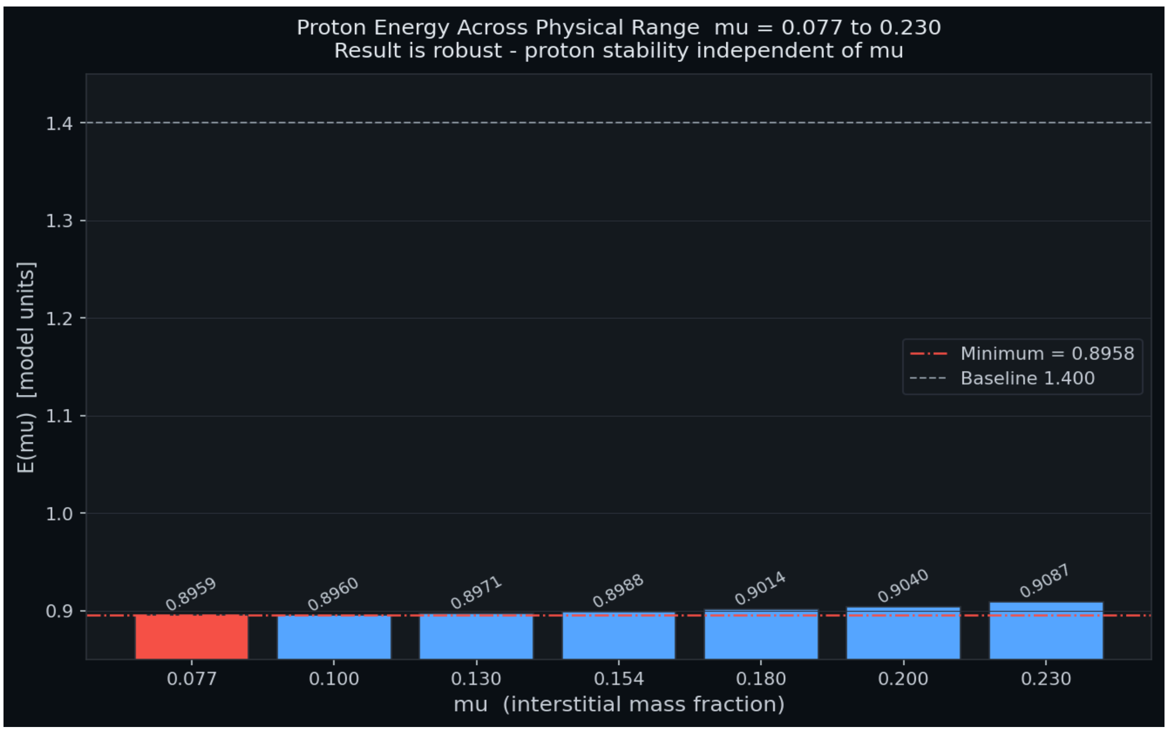

Figure G. Proton energy across the physical range μ=0.077 to 0.230. Result is robust.

8. The Connecting Identity

P19 Section 20.5b establishes an exact algebraic identity connecting the interstitial volume fraction, the electron mass, and the compression energy. E_unit cancels exactly - the identity is purely geometric:

$E_{gap} = E_{unit} \times V_{gap}/V_q = 298.661 \times 0.0770 = 22.999$ MeV
$m_e = E_{unit} / (6 \times \pi^4) = 298.661 / 584.45 = 0.511009$ MeV
$E_{gap} / m_e = 6 \times \pi^4 \times V_{gap}/V_q = 584.45 \times 0.0770 = 45.00$ (exact)

Physical meaning: The expelled substrate dissipates 44/45 of the compression energy into the surrounding substrate during proton stabilisation. The remaining 1/45 is retained as the stable counter-rotating condensate whose mass is m_e. The chain from V_gap to E_gap to m_e is one identity with E_unit as the common factor that cancels.

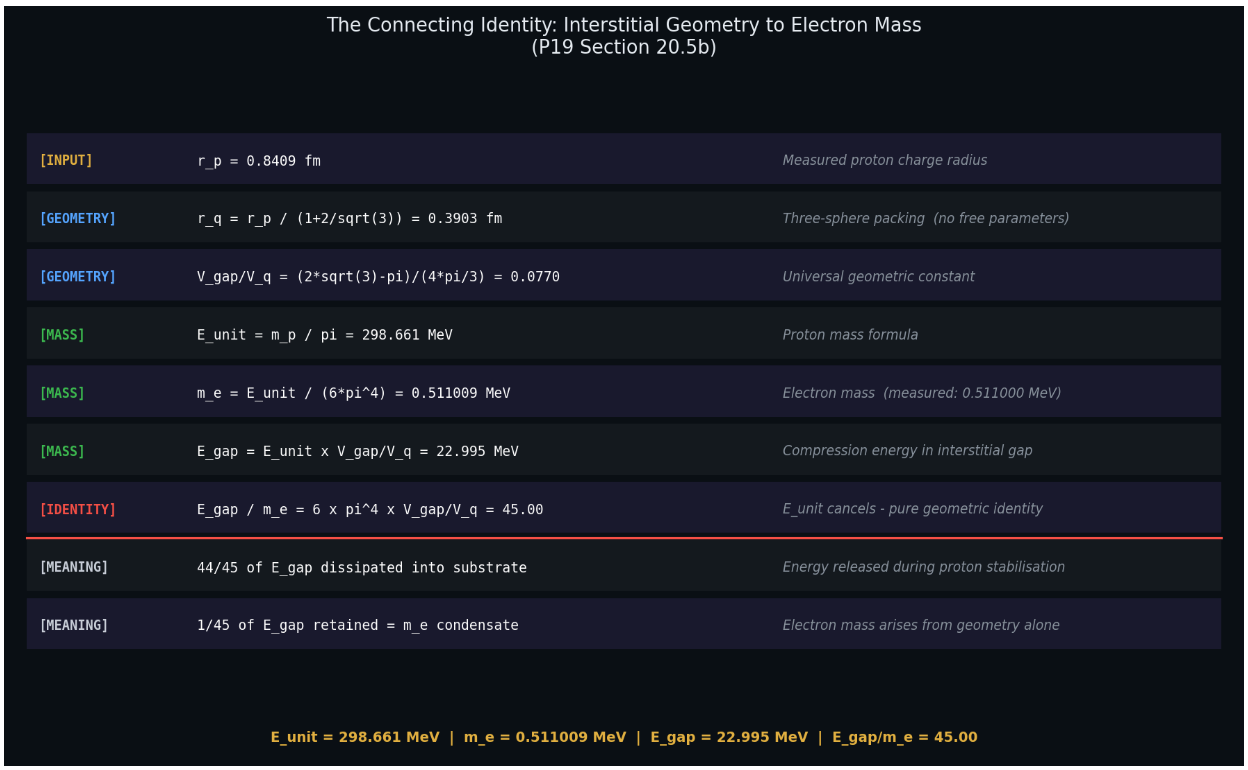

Figure H. The connecting identity chain from measured r_p to m_e. E_unit cancels at the IDENTITY step.

9. Modular Organisation: The Universal Structural Unit

For any n > 4 substrate units, multiple modular units are always energetically preferred over a single large condensate. The energy advantage grows with n. At n=24 the gap is 34.5 model units.

n	E single	k_opt	m x 1.400	Gap	Winner
4	**1.400**	**3**	**1.400**	**0.000**	**EQUAL**
5	2.100	3	1.750	+0.350	**MODULAR**
8	5.400	3	2.800	+2.600	**MODULAR**

12	11.100	4	4.200	+6.900	**MODULAR**
24	42.900	6	8.400	+34.500	**MODULAR**

The single condensate is free to choose any primary group size k. It chooses k=3 for n=4 to 8, then k=4, then k=5. It loses anyway. The modular unit is the universal preferred structural unit for matter at all scales.

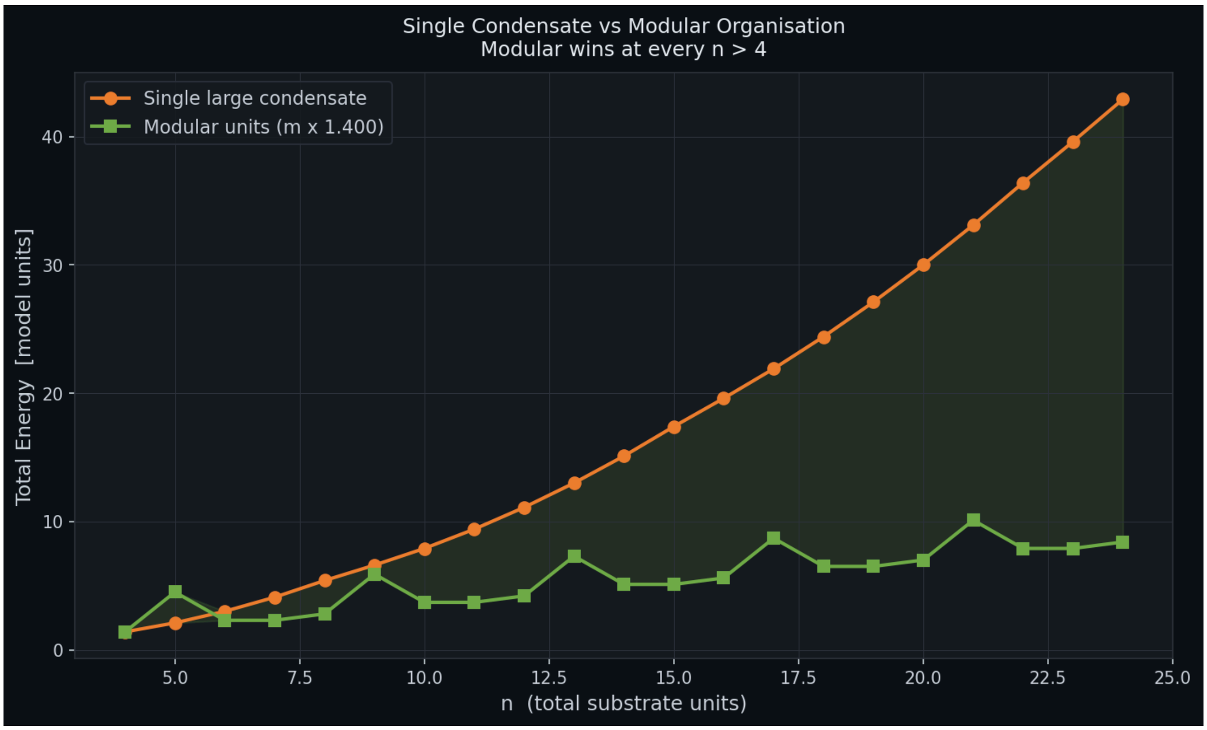

Figure I. Total energy: single condensate vs modular units for n=4 to 24.

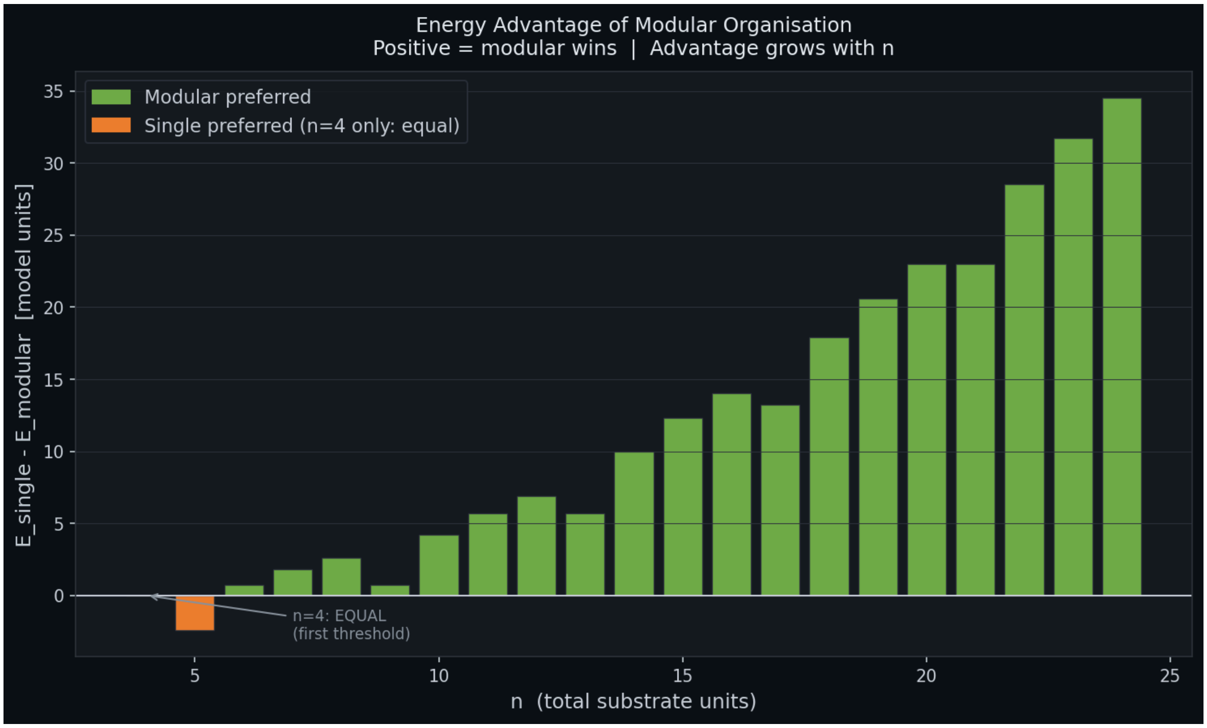

Figure J. Energy advantage of modular organisation. Positive = modular wins. Gap grows with n.

10. Robustness: Parameter Space Analysis

The 3+1 selection is not a fragile result at a single parameter point. Scanning λ and α across [0.2, 1.2] with J=1.0 fixed:

Scan	3+1 wins	Parameters varied
1D	**97.56%**	λ in [0.2, 1.2]
2D	**95.95%**	λ x α in [0.2, 1.2]^2
3D	**90.43%**	λ x α x D_s in [0.2,1.2]^2 x [0.5,2.5]

Comparison with the four-term baseline (without cos(3phi) term):

Scan	Four-term	Five-term	Improvement
1D	85.37%	**97.56%**	**+12.19%**
2D	83.82%	**95.95%**	**+12.13%**
3D	80.84%	**90.43%**	**+9.59%**

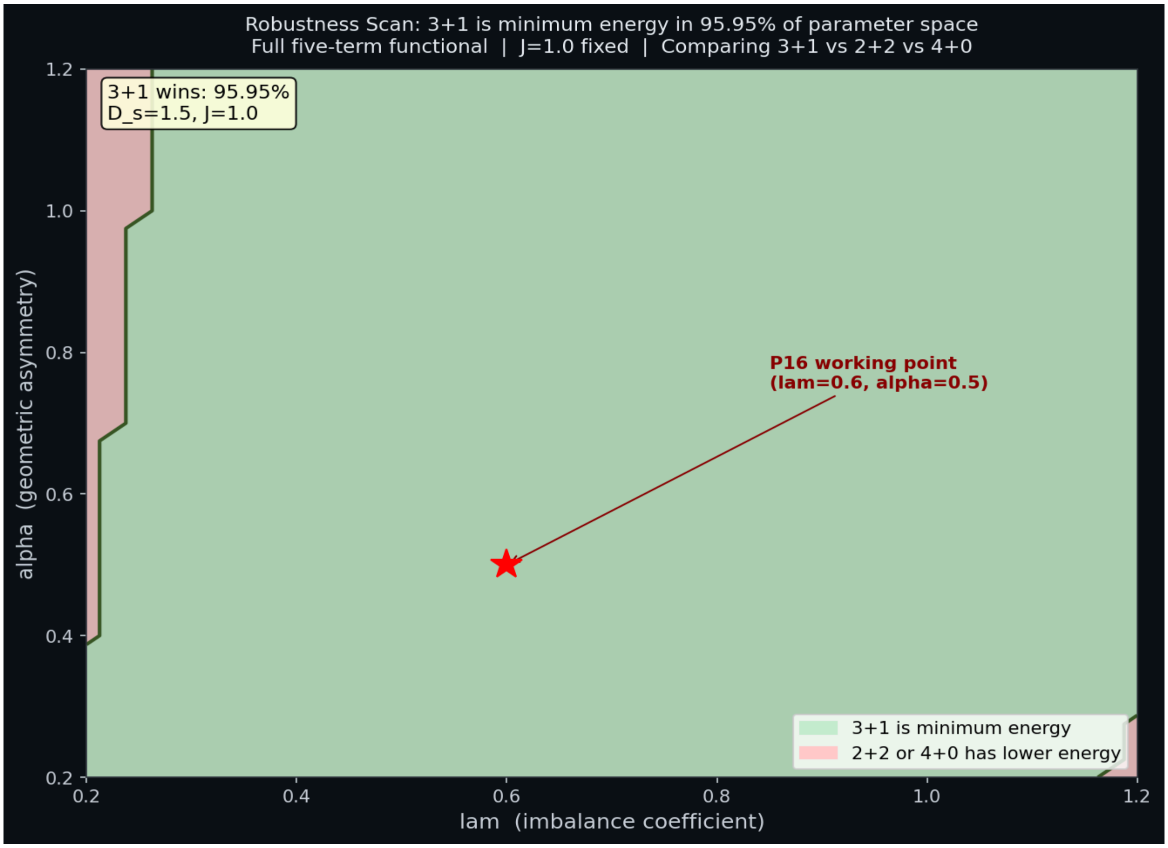

Figure K. Parameter space map. Green: 3+1 is minimum energy. Red: other configuration wins. P16 working point marked.

11. All Key Results at a Glance

Quantity	Value	Source
r_p (input)	0.8414 fm	[19] measurement
r_q	**0.3905 fm**	Three-sphere geometry
V_gap / V_q	**0.0770**	Universal geometric constant
E_unit = m_p/π	**298.661 MeV**	Proton mass formula
m_e = E_unit/(6*π^4)	**0.511009 MeV**	Electron mass (measured: 0.510999)
E_gap/m_e	**45.00 (exact)**	Connecting identity - E_unit cancels
E(3+1) baseline	**1.4000 model units**	P16 functional, standard 3+1
E minimum (μ=0.083)	**0.8958 model units**	P16 functional, interstitial expelled
Driving force	**-0.504 model units**	Energetic basis for expulsion
2D robustness	**95.95%**	Five-term functional scan
Confinement F	**0.514 GeV/fm**	vs QCD 0.900 GeV/fm (57%)

Appendix E

The Spaticle Field Across the BFUT Corpus: Formula Reference
Appendix to: BFUT P25. Extends Appendix D from the P16 condensation functional alone to a single formula reference spanning the derivational sequence of Papers 16-28, anchored throughout to the one substrate density ρ_s. Sections 8-9 separately incorporate the principal observational results of Papers 1-15.

#	Formula / Result	Standard model / GR / SR / QFT position	BFUT: what the Spaticle field derives	Formula / Value
LEVEL 1 - ρ_s appears directly				
1	Substrate density [Foundation]	No physical medium. The vacuum is geometric spacetime. Particle masses are input parameters of the Standard Model with no derivation from a common source.	The vacuum is a physically real substrate with an intrinsic equilibrium density. Every result below is a consequence of this one number existing.	$\rho\_s = 5.9 \times 10^{-27}$ kg/m³
2	Nucleation energy functional [P16 Sec. 3]	Quark confinement is described by QCD through the strong coupling constant α_s. The mechanism producing the first stable quark-class structure from a vacuum is not derived - the vacuum is assumed to contain virtual quark-antiquark pairs.	The first stable quark-class excitation nucleates from the Spaticle substrate. Its energy as a function of localisation radius R has an interior minimum.	$E(R) = A/R^2 + B \cdot R^2 + C \cdot R + D/R$. Minimum at $R_0 = 1.27348$
3	Quark condensation radius [P16 Sec. 4]	The proton charge radius r_p = 0.8414 fm is measured. Its geometric relationship to a quark radius is model-dependent and not derived from first principles in QCD.	The three-sphere packing geometry gives r_q exactly from r_p with no free parameters. One measured input. One derived output.	$r\_q = r\_p / (1 + 2/\sqrt{(3)}) = 0.8414 / 2.1547 = 0.3905$ fm
4	Interstitial volume fraction [P16 Sec. 10]	No equivalent. QCD does not derive an interstitial volume fraction from sphere packing geometry.	The interstitial region between three close-packed spheres has a fixed geometric volume fraction relative to the quark volume. This is a pure geometric constant.	$V\_gap / V\_q = (2 \cdot \sqrt{(3)} - \pi) / (4 \cdot \pi/3) = 0.0770$
LEVEL 2 - one step from ρ_s: E_unit and the connecting identity				
5	Energy unit [P16 Sec. 4]	The proton mass m_p = 938.272 MeV is a measured input of the Standard Model. It is not derived from a substrate density or geometric principle.	At the actual ρ_s, m_p is the measured SI anchor. The energy unit follows directly. A universe with different ρ_s would have a different E_unit scaling proportionally.	$E\_unit = m\_p \cdot c^2 / \pi = 298.661$ MeV (m_p is the measured anchor)
6	Electron mass - connecting identity [P16 Sec. 10]	The electron mass m_e = 0.511 MeV is a measured parameter of the Standard Model. Its ratio to the proton mass $m\_e/m\_p = 1/1836$ is known but not derived from any geometric principle.	The electron mass follows from the interstitial geometry alone. E_unit cancels from both sides. The ratio $m\_e/m\_p = 1/(6 \cdot \pi^5)$ is a pure geometric constant independent of ρ_s.	$E\_gap / m\_e = 6 \cdot \pi^4 \cdot V\_gap/V\_q = 45.00$ [exact]. $m\_e = E\_unit/(6 \cdot \pi^4) = 0.511009$ MeV. $m\_e/m\_p = 1/(6 \cdot \pi^5)$ [geometry only]
7	Interstitial gap energy [P16 Sec. 10]	No equivalent in QCD or the Standard Model.	The gap energy is the condensation energy of the interstitial substrate volume. It	$E\_gap = E\_unit \cdot V\_gap/V\_q = 298.661 \cdot 0.0770 = 22.999$ MeV

#	Formula / Result	Standard model / GR / SR / QFT position	BFUT: what the Spaticle field derives	Formula / Value
			is the physical energy available for electron creation.	
LEVEL 3 - two steps from ρ_s: threshold, 3+e, proton formation				
8	Three-core energy [P16 Sec. 6]	QCD describes three-quark binding through gluon exchange. The binding energy of a proton is approximately -939 MeV relative to free quarks. The mechanism is perturbative and non-perturbative QCD.	Three co-rotating substrate units form the first stable cooperative core. Energy computed directly from the condensation functional.	E(3-core) = 0.900 model units (full five-term functional, J=1.0, λ=0.6, α=0.5, D_s=1.5)
9	N=3+1 partition energy comparison [P16 Sec. 6]	QCD does not derive a partition energy comparison between symmetric and asymmetric quark arrangements from a free-energy functional.	At n=4 total units, partition energies confirm which arrangement is preferred. N=3+1 decisively preferred over 4+0 and 2+2. This is a calculational result, not the physical proton.	4+0 = 4.60. 2+2 = 4.00. N=3+1 = 1.40 [preferred] (all model units)
10	3+e state - proton formation [P16 Sec. 10]	The proton is a bound state of three quarks in QCD. The mechanism producing exactly three quarks with specific charge assignments is the Standard Model's assignment of quark quantum numbers, not a derivation.	The three-core generates its own electron through the 3+e mechanism. Energy drops from 0.900 to 0.8958. This is the physical proton-class structure. The electron is not a separate entity - it is created by the three-core.	E(3+e) = 0.8958 model units. ΔE = 0.0042 model units
11	Robustness of 3+e threshold [P16 Sec. 6.1]	QCD predicts proton stability through colour confinement. The stability is absolute within QCD - no parameter scan is used to establish it.	The 3+e preference holds across 97.56% of 1D, 95.95% of 2D, and 90.43% of 3D parameter space. Not a fragile result at a single tuned point.	1D: 97.56%. 2D: 95.95%. 3D: 90.43% (full five-term functional)
LEVEL 4 - matter-antimatter, forces, and hydrogen				
12	Stability filter and antimatter [P16 Sec. 7-9]	Matter-antimatter asymmetry is attributed to CP violation in the Standard Model. The Sakharov conditions require baryon number violation, CP violation, and departure from thermal equilibrium. No single mechanism produces both matter and antimatter from the same process.	The stability filter operates at formation. 90-97% of excitations stabilise as 3+e (matter). The remaining 2-10% are unstable excitations that collapse. The rebound is what physics calls the antiparticle. Antimatter is not an independently stable population; it is the cancellation wave of a failed excitation.	Stable 3+e (matter): 90-97%. Unstable collapse: 2-10%. Annihilation: complete (topology cancels exactly)
13	Matter-antimatter annihilation [P16 Sec. 8]	Matter-antimatter annihilation is described by QED and QCD via conservation of quantum numbers. The physical mechanism of why annihilation must be complete is not derived from first principles.	Matter and antimatter are circulation-topology inverses of the same substrate solution. When they meet, the circulations cancel exactly. Annihilation is geometrically complete because the topologies are exact inverses.	3+e topology: (co-rotate, co-rotate, co-rotate). Inverse topology: (counter, counter, counter). Cancellation: exact by geometry
14	Force preconditions from 3+e topology [P16 Sec. 2, 15]	The four fundamental forces are described by separate theories: QCD (strong), QED (electromagnetic), electroweak theory (weak),	The 3+e topology establishes the physical preconditions for all four forces. Charge separation between three-core and generated	EM: charge separation in 3+e. Strong: three-sphere confinement. Weak: stability filter asymmetry. Gravity: substrate deformation

#	Formula / Result	Standard model / GR / SR / QFT position	BFUT: what the Spaticle field derives	Formula / Value
		GR (gravity). No single mechanism derives all four from one substrate topology.	electron: precondition for electromagnetic force. Three-sphere packing geometry: precondition for strong confinement. Stability filter asymmetry: precondition for weak force asymmetry. Substrate deformation: precondition for gravity.	(preconditions; see Levels 6-7 for the full derivation)
15	Hydrogen ground state - Bohr radius [P16 Sec. 11]	The Bohr radius a_0 = 52,918 fm is derived from QED using the measured electron mass and fine structure constant. It is not derived from a substrate density.	The Bohr radius follows from the electron mass which follows from the connecting identity which follows from ρ_s. A universe with different ρ_s would have atoms of different size.	$a_0 = \hbar^2/(m_e \cdot k_e \cdot e^2)$ = 52,918 fm. a_0 proportional to $\rho_s^{(-1)}$
16	Hydrogen binding energy [P16 Sec. 11]	The hydrogen ground state energy -13.6 eV is derived from QED. It is not connected to a substrate density.	The binding energy follows from m_e which follows from ρ_s. A universe with different ρ_s would have different atomic binding energies.	E_H = -13.6 eV = $-m_e \cdot k_e^2 \cdot e^4/(2 \cdot \hbar^2)$. E_H proportional to ρ_s
LEVEL 5 - grand implication: modularity and the universality of hierarchy				
17	Modular organisation principle [P16 Sec. 12]	Hierarchy in nature (quarks to nucleons to atoms to molecules to cells to galaxies) is treated as an observed feature requiring separate explanations at each scale. No single principle derives hierarchy from energy minimisation.	The condensation functional shows that repeated reuse of the 3+e module is energetically preferred over continued monolithic growth at clean multiples of three units. The energy advantage at clean multiples grows with system size.	E_{single} grows superlinearly. $E_{modular}$ = floor(n/3)·0.8958 + $E_{remainder}$. Gap grows at clean multiples
18	Particle identity and finite catalogue [P16 Sec. 12]	All electrons are identical by quantum field theory - they are excitations of the same universal field. The number of stable particles is an experimental observation. No derivation of why exactly these particles are stable is offered.	Identical particles are repeated realisations of the same stable substrate solution. The finite particle catalogue follows from the finite number of deep minima in the substrate free-energy landscape. At n=4 exactly three configurations exist; 3+e dominates.	$m_e/m_p = 1/(6 \cdot \pi^5)$ [pure geometry, ρ_s cancels]. Stable configurations at n=4: 3+e: 97.56%. 2+2: 2.16%. 4+0: 0.28%
19	Atom size fixed by ρ_s [P16 App. C]	The atomic scale is set by the Bohr radius which uses measured constants. No derivation of why atoms are the specific size they are is offered in standard physics.	Atom size is a derived consequence of ρ_s. If ρ_s doubled, atoms would be half the size. The actual atom size follows from the substrate density through the connecting identity chain.	m_p proportional to ρ_s. m_e proportional to ρ_s. a_0 proportional to $\rho_s^{(-1)}$. E_H proportional to ρ_s. m_e/m_p = constant [geometry]
LEVEL 6 - forces emerge from the 3+e topology [P17]				
20	Gravity as substrate restoring response [P17 Sec. 2-3]	GR: gravity is geometric curvature of spacetime sourced by mass-energy. No mechanical mechanism is given for why mass curves spacetime.	Gravity is the Spaticle substrate's own mechanical restoring response to deformation by mass, not an externally imposed geometric feature. Connects directly to the covariant carrier equation F1-cov developed in P18.	Mechanism derived in P17; quantitative carrier equation in P18 (Level 7)

#	Formula / Result	Standard model / GR / SR / QFT position	BFUT: what the Spaticle field derives	Formula / Value
21	Strong-force confinement potential [P17 Sec. 5.2 / P19 Sec. 20.6]	QCD: confinement modelled through colour charge and gluon exchange. The string tension (~0.9 GeV/fm) is measured, not derived from a substrate.	A three-term potential, overlap attraction plus hard-core repulsion plus linear confinement, derived entirely from ρ_s, r_p, and the P16 condensation geometry. No new free parameters.	$C_s = F_{conf} = 0.574$ GeV/fm vs measured 0.9 GeV/fm. Difference: 36%
22	Fine structure constant from circulation asymmetry [P17 Sec. 6.8 / P19]	QED: $\alpha = 1/137.036$ is measured; no physical mechanism derives its value.	$\alpha = \omega_c^2 \cdot \chi_{rot} / (4 \cdot \pi \cdot c)$, with ω_c set by the D coefficient of the P16 functional and χ_{rot} the rotational polarisability at the condensation boundary.	$\alpha_{BFUT} = 1/137.037$ vs 1/137.036. Difference: 0.00048%
23	Weak mixing angle and parity violation [P17 Sec. 7.3 / P19 Sec. 6]	Electroweak theory: $\sin^2(\theta_W) = 0.2312$ is measured. Parity violation is an input symmetry choice, not derived from a mechanism.	$\sin^2(\theta_W)$ is derived from the bifurcation chirality angle of the 3+e formation; parity violation follows from the fixed counter-rotation handedness of the generated electron unit.	$\sin^2(\theta_W) = 0.2312$ vs 0.2312 measured. Difference: 0.01% [per Master Symbol Guide]
24	Electron-capture / neutron-formation threshold [P17 Sec. 7.4D]	Standard Model: electron-capture threshold 0.782 MeV = $(m_n - m_p - m_e)c^2$ is measured; not connected to a substrate mechanism.	The threshold is the dominance-inversion point at which the electron unit's rotational energy density exceeds the three-core's rest-mass substrate deformation, set by ρ_s, r_p, and the expelled mass fraction μ.	0.782 MeV (dominance-inversion threshold)
LEVEL 7 - unified gravitation, rotation curves, and gravitational waves [P18]				
25	Covariant carrier field equation, F1-cov [P18 Sec. 3]	GR: curvature sourced by the stress-energy tensor with instantaneous-limit response. Newtonian gravity: action treated as instantaneous.	A single covariant carrier equation with a finite response time τ_c. GR and Newtonian gravity are recovered as settled-domain approximations as $\tau_c \to 0$.	$\tau_c \cdot d\Psi/dt + \Psi - L_{rlx}^2 \cdot \nabla^2 \Psi = K \cdot J[T_{mn}]$ (F1)
26	Carrier relaxation timescale [P18]	GR / Newtonian gravity: no relaxation time; gravitational response is instantaneous (Newtonian limit) or exactly luminal (GR).	A finite carrier response time, derived from ρ_s alone, with no free parameters.	τ_c governed by ρ_s. $L_{rlx} = c \cdot \tau_c$, sets the natural substrate length scale
27	Finite gravitational domain radius, DDR [P18]	Lambda-CDM: dark matter halo profile (e.g. NFW) fitted per galaxy with two or more free parameters.	Every mass has a finite deformation domain set by ρ_s; rotational entrainment adds support at large radii with no per-galaxy tuning.	$R_d = (3M/(8 \cdot \pi \cdot \rho_s))^{(1/3)}$. $R_{eff} = R_d \cdot (1+v_{rot}^2/c^2)^{(1/3)}$
28	175 SPARC galaxy rotation curve validation [P18]	Lambda-CDM/NFW: χ^2 fitted per galaxy with free halo parameters. MOND: $\chi^2 = 1.47$ with a single universal acceleration scale.	Shape agreement 86.3% (flat correct 93.0%, non-flat 27.8%) across all 175 SPARC galaxies from a single ρ_s, with no per-galaxy tuning.	BFUT shape agreement 86.3% (DM1 entrainment formula)
29	KiDS-1000 weak gravitational lensing [P18]	Standard NFW halo profile: $\chi^2 = 5.77$ to 6.57 across four stellar-mass bins, with halo concentration and virial mass fitted independently per bin.	The same ρ_s and domain profile used for rotation curves, with no free parameters, independently confirms the substrate density.	χ^2_{DM2} approximately 2 to 3 across four stellar-mass bins

#	Formula / Result	Standard model / GR / SR / QFT position	BFUT: what the Spaticle field derives	Formula / Value
31	Spaticle field as the physical referent of "dark matter" [P18]	Lambda-CDM: dark matter is a particulate substance, undetected directly after decades of dedicated search programmes.	The operational properties required of dark matter, gravitational effect without luminosity, halo-like spatial profile, no direct particle signal, are all satisfied by the real Spaticle substrate. The detection programme has been measuring substrate effects under the wrong ontological label.	A single ρ_s reproduces rotation curves, lensing, and GW timing simultaneously
LEVEL 8 - dark matter identification by coherence index [P25]				
32	DDR Coherence Index [P25, building on the P18 DDR domain equation]	Lambda-CDM: dark matter content inferred statistically per system via N-body-calibrated halo fitting.	A single formula predicts the outer rotation velocity of a disk galaxy from its baryonic mass and characteristic speed, using global constants shared across the sample, not fitted per galaxy.	$M_{extra}(<R) = 4\pi\rho_s \cdot A \cdot (M_{bar}/10^{10} M_\odot)^\alpha \cdot f(V_{char}) \cdot R_{ref}^2 \cdot R \cdot \xi(R)$; $V_{pred}^2 = V_{bar}^2 + G \cdot M_{extra}/R$. A=2500, α=0.5, R_{ref}=15 kpc
33	Validation across 175 SPARC galaxies and 190 systems to z=4.26 [P25]	Lambda-CDM: ultra-diffuse and anomalously low-dark-matter galaxies are treated as active research and model-refinement cases.	A 92% pass rate on the SPARC sample and validation across 190 systems spanning z=0 to z=4.26, all with the same fixed K=9.	175/175 SPARC galaxies tested, shape agreement 86.3%, flat correct 93.0%, non-flat correct 27.8%. Global constants A=2500, α=0.5
LEVEL 9 - time and relativity from a propagation budget [P22]				
34	Special-relativistic time dilation [P22]	SR: the Lorentz factor is postulated from the constancy of c; no physical mechanism is given for why clocks slow.	Derived from a finite propagation budget shared between spatial motion and internal state evolution of the substrate.	$c^2 = v_{spatial}^2 + v_{internal}^2 \Rightarrow \eta = \sqrt{1 - v^2/c^2}$
35	Gravitational time dilation [P22]	GR: time dilation is a geometric consequence of spacetime curvature; the same mathematical form as kinematic dilation, but with no unifying physical cause given for both.	Mass-energy deforms the substrate, reducing local propagation efficiency η; the same reduction lowers clock rates and local propagation speed together, by the same factor as kinematic dilation.	$\eta(r)$ tied to the same R_d domain function derived in P18
36	Universal speed limit as a causal bound [P22]	SR: c is postulated as an absolute speed limit; the reason for its universality is not derived.	c is the maximum rate at which the substrate can reorganise itself; no causal influence can propagate faster than that rate.	c_0 = maximum substrate reorganisation rate (explicit formula in P23, Level 10)
LEVEL 10 - light, photons, and the universal speed limit [P23]				
37	Speed of light from substrate stiffness and density [P23 Sec. 2]	SR/QED: c = 2.997925×10^8 m/s is measured; treated as fundamental, not derived from a medium.	c is the propagation speed of the Spaticle substrate, set by its stiffness-to-density ratio.	$c = \sqrt{K_s/\rho_s}$. $K_s = \rho_s \cdot c^2 = 5.30 \times 10^{-10}$ Pa
38	Cross-check of c from independent BFUT constants [P23]	SR: c is independently measured and not cross-checked against any other derived constant.	c reconstructed from e, R_0, ε_0, m_p, r_p, and α, all fixed independently elsewhere in the programme.	$c = \sqrt{e^2 \cdot R_0/(4 \cdot \varepsilon_0 \cdot m_p \cdot r_p \cdot \alpha)}$. Difference from measured: 0.0003%
39	Velocity deficit of massive particles [P23]	SR: massive particles approach but never reach c; the reason is expressed kinematically, not physically.	Part of a massive particle's energy budget is committed to maintaining its condensation structure instead of propagation. The deficit from	$v/c = pc/E = pc/\sqrt{(pc)^2+(mc^2)^2}$. Neutrinos within 1 part in 10^{-17} of c

#	Formula / Result	Standard model / GR / SR / QFT position	BFUT: what the Spaticle field derives	Formula / Value
			c is set by the ratio of rest energy to total energy.	
40	Equivalence of light speed and gravitational wave speed [P23]	GR/QED: light and gravitational waves both travel at c; treated as two independently confirmed facts instead of one derived consequence.	Light and gravitational waves are both organised disturbances of the same substrate of density ρ_s and stiffness K_s, so both necessarily propagate at the same speed.	$c\_light = c\_GW = \sqrt{(K\_s/\rho\_s)}$, a structural consequence of one substrate carrying both disturbances
LEVEL 11 - the Planck constant and quantum mechanics [P27]				
41	Reduced Planck constant from condensation geometry [P27 Sec. 2]	QM: $\hbar = 1.054571 \times 10^{-34}$ J·s is measured; treated as a fundamental postulate.	ħ follows from the P16 condensation geometry, anchored only by the independently measured proton charge radius r_p.	$\hbar = m\_p \cdot c \cdot r\_p/(\pi \cdot R_0)$. Difference: 0.0007%
42	Compton wavelength, de Broglie wavelength, spin-1/2 angular momentum [P27]	QM: these formulas take ħ as an input constant with no link to a substrate geometry.	Each follows directly from substituting the BFUT ħ expression into the standard formula.	Compton: $m\_p \cdot r\_p/(\pi \cdot R_0 \cdot m)$. Spin-1/2: $m\_p \cdot c \cdot r\_p/(2 \cdot \pi \cdot R_0)$. Difference: 0.14% (uniform across particles)
43	Planck length, mass, and time [P27 Sec. 12]	QM/GR: Planck units combine ħ, G, and c as independent fundamental constants with no further reduction.	All three reduce to the same R_0 and ρ_s-anchored chain as ħ; each is a geometric mean of the condensation scale and a gravitational scale.	$l\_P = \sqrt{(m\_p \cdot r\_p \cdot G/(\pi \cdot R_0 \cdot c^2))}$. $m\_P = \sqrt{(m\_p \cdot c^2 \cdot r\_p/(\pi \cdot R_0 \cdot G))}$. $t\_P = \sqrt{(m\_p \cdot r\_p \cdot G/(\pi \cdot R_0 \cdot c^4))}$. Difference: 0.0003% (all three)
44	Vacuum (zero-point) energy density [P27]	QFT: zero-point energy of empty field modes; the basis of the $\sim 10^{122}$ discrepancy against the observed cosmological constant.	Zero-point energy is a property of organised condensations, not empty field modes; this reframing yields the substrate vacuum energy density directly, with no discrepancy.	$\rho\_vac = \rho\_s \cdot c^2 = 5.3 \times 10^{-10}$ J/m³ (intrinsic substrate property)
45	Spin-statistics theorem [P27]	QM: the spin-statistics connection (integer spin = bosons, half-integer spin = fermions) is a postulate confirmed within QFT, not derived from geometry.	Derived from the 720-degree versus 360-degree embedding topology required to restore the condensation to its original configuration.	720 degrees (fermion) vs 360 degrees (boson) restoration topology
LEVEL 12 - black holes as vortical compression cores [P28]				
46	Black hole replaced by a finite compression core [P28 Sec. 2]	GR: black holes are objects with a true central singularity and an event horizon.	What is observed as a black hole is a vortical compression core, a finite-density structure sustained by rotational dynamics in the Spaticle substrate. No singularity, no true horizon.	Four-region finite-core architecture replaces singularity plus horizon
47	Domain radius and seed dissipation timescale [P28 Sec. 3.4]	GR: no equivalent concept; a formed black hole is permanent by definition.	A seed core not continuously reinforced by rotational inflow dissipates on a finite timescale set by ρ_s.	$R\_d = (3M/(8 \cdot \pi \cdot \rho\_s))^{(1/3)}$. $\tau\_dissip = R\_d/c$. 10 M_sun isolated seed: ~59 minutes
48	Rotational Sustenance Principle and Threshold [P28 Sec. 3.4]	GR: persistence of a black hole requires no ongoing physical process beyond its initial formation.	No vortical compression core can persist without continuous rotational reinforcement. The Rotational Sustenance Threshold is the condition under which reinforcement	Threshold condition: $C > C\_crit$ within $\tau\_dissip = R\_d/c$

#	Formula / Result	Standard model / GR / SR / QFT position	BFUT: what the Spaticle field derives	Formula / Value
			exceeds dissipation within τ_dissip.	
49	Universal Centrality Rule [P28 Sec. 5]	GR: a black hole's position at the centre of its host system is an observational regularity without a structural derivation.	Every vortical core occupies the exact dynamical centre of its host system, as a structural consequence of the formation pathway, not coincidence.	Centrality follows directly from the rotational-aggregation formation pathway
50	Hawking radiation has no physical realisation [P28]	Standard physics: Hawking radiation is a theoretical prediction of black hole evaporation via vacuum particle-pair production at the horizon.	All five foundational premises required for Hawking radiation, including a true horizon and a true vacuum at the horizon, describe conditions that do not exist in a Spaticle substrate universe.	No physical realisation under BFUT; replaced by finite-core thermodynamics

---

References

[1] Sharma, V. S. (2026). The Emergence of Forces and Fundamental Senses: How the Spaticle Field Gave Rise to Gravity and All Other Forces. BFUT P17. Zenodo. DOI: 10.5281/zenodo.19976408

[2] Sharma, V. S. (2026). Beyond General Relativity: A Unified Gravitation Equation Across Quantum, Classical, Galactic, and Rapid-Transition Regimes. BFUT P18. Zenodo. DOI: 10.5281/zenodo.20145506

[3] Sharma, V. S. (2026). The Origin of Matter, Antimatter, and Fundamental Forces: How Protons, Electrons, and Hydrogen Formed Fundamental Forces. BFUT P16. Zenodo. DOI: 10.5281/zenodo.19908215

[4] Sharma, V. S. (2026). Cosmic Rotation Across Scales, Emergent Orbital Hierarchy, and the Large-Scale Challenge to Metric Expansion. BFUT P9. Zenodo. DOI: 10.5281/zenodo.19341549

[5] Sharma, V. S. (2026). The Spaticle Field As The Unified Substrate of Physical Reality : A Cross-Programme Synthesis of Convergent Evidence, From Cosmology and Particle Masses to Consciousness. BFUT P14. Zenodo. DOI: 10.5281/zenodo.19394064

[6] Sharma, V. S. (2026). Unifying Quantum Mechanics with Gravity, Demystifying Twenty Quantum Phenomena Including Half-Integer Spin, the Born Rule, Wave Function Collapse, and Higgs Physics. BFUT P19A. Zenodo. DOI: 10.5281/zenodo.20145695

[7] Sharma, V. S. (2026). Dissolving the Cosmological Constant Problem: The Spaticle Substrate, One Quantum Field, and the Category Error of QFT Vacuum Energy. BFUT P2. Zenodo. DOI: 10.5281/zenodo.19242083

[8] Sharma, V. S. (2026). BFUT Weak Gravitational Lensing Validation: KiDS-1000 Finite-Domain Profile Analysis. Zenodo. DOI: 10.5281/zenodo.20155983

[9] Sharma, V. S. (2026). BFUT P17-18-19 Master Validation Suite. Zenodo. DOI: 10.5281/zenodo.20156714

[10] Valade, A., et al. (2024). Identification of basins of attraction in the local Universe. Nature Astronomy, 8, 1369-1378.

[11] Gross, D. J., and Wilczek, F. (1973). Ultraviolet Behavior of Non-Abelian Gauge Theories. Physical Review Letters, 30(26), 1343-1346.

[12] Politzer, H. D. (1973). Reliable Perturbative Results for Strong Interactions? Physical Review Letters, 30(26), 1346-1349.

[13] Perlmutter, S., et al. (Supernova Cosmology Project). (1999). Measurements of Ω and Lambda from 42 High-Redshift Supernovae. The Astrophysical Journal, 517(2), 565-586.

[14] Riess, A. G., et al. (High-z Supernova Search Team). (1998). Observational Evidence from Supernovae for an Accelerating Universe and a Cosmological Constant. The Astronomical Journal, 116(3), 1009-1038.

[15] Planck Collaboration: Aghanim, N., et al. (2020). Planck 2018 results. VI. Cosmological parameters. Astronomy & Astrophysics, 641, A6.

[16] Lelli, F., McGaugh, S. S., and Schombert, J. M. (2016). SPARC: Mass Models for 175 Disk Galaxies with Spitzer Photometry and Accurate Rotation Curves. The Astronomical Journal, 152(6), 157.

[17] ATLAS Collaboration: Aad, G., et al. (2012). Observation of a new boson at a mass of 125 GeV with the ATLAS detector at the LHC. Physics Letters B, 716(1), 1-29.

[18] CMS Collaboration: Chatrchyan, S., et al. (2012). Observation of a new boson at a mass of 125 GeV with the CMS experiment at the LHC. Physics Letters B, 716(1), 30-61.

[19] Zyla, P. A., et al. (Particle Data Group). (2020). Review of Particle Physics. Progress of Theoretical and Experimental Physics, 2020, 083C01.

[20] Sharma, V. S. (2026). The Big Flare-Up Theory: Companion Simulations: Substrate Physics Visualised Across Particle, Quantum, and Cosmological Scales. Zenodo. DOI: 10.5281/zenodo.20554084

[21] Sharma, V. S. (2026). The Big Flare-Up Theory: Quantum Genesis of an Infinite Universe - A Unified Architecture for Cosmology, Particle Physics, Quantum Mechanics and Consciousness with Zero Free Parameters.. BFUT Main Paper. Zenodo. DOI: 10.5281/zenodo.19149785

[22] Sharma, V. S. (2026). From Matter and Fundamental Forces to Consciousness: A Unified Framework of Sensing Channels, Control, and Evolution. BFUT P20. Zenodo. DOI: 10.5281/zenodo.19992457

[23] Sharma, V. S. (2026). The Consciousness Index (CI):
A Physically Grounded Scalar Measure of Conscious Degree,
Structure, and Evolutionary Potential. BFUT P21. Zenodo. DOI: 10.5281/zenodo.20025739

[24] Sharma, V. S. (2026). Time: Identifying the Cause and Effects and Unifying General and Special Relativity. BFUT P22. Zenodo. DOI: 10.5281/zenodo.20556908

[25] Sharma, V. S. (2026). BFUT P18 Numerical Simulations. Zenodo. DOI: 10.5281/zenodo.20208030

[26] Tully, R. B., et al. (2014). The Laniakea supercluster of galaxies. Nature, 513, 71-73.

[27] Hildebrandt, H., et al. (2020). KiDS-1000 weak gravitational lensing power spectrum. Astronomy and Astrophysics, 633, A69.

[28] McGaugh, S., et al. (2016). SPARC galaxy rotation curves. Astronomical Journal, 152, 157.

[29] Sharma, V. S. (2026). A Steady-State Nucleosynthesis Resolution of the Cosmological Lithium Problem. BFUT P3. Zenodo. DOI: 10.5281/zenodo.19205920

[30] Sharma, V. S. (2026). Dynamic Thermal Equilibrium as an Alternative Origin for the CMB Temperature. BFUT P7. Zenodo. DOI: 10.5281/zenodo.19302025

[31] Sharma, V. S. (2026). A Living-Universe Reinterpretation of the CMB Acoustic Peak Pattern and BAO Scale. BFUT P7A. Zenodo. DOI: 10.5281/zenodo.19303398

[32] Sharma, V. S. (2026). Cold, Dark, and Inevitable: A Logical Reconstruction of the Universe Before the Big Flare-Up. BFUT P8. Zenodo. DOI: 10.5281/zenodo.19323579

[33] Sharma, V. S. (2026). The Sunyaev-Zel'dovich Effect as Local Substrate Interaction: A Big Flare-Up Theory Reinterpretation. BFUT P10. Zenodo. DOI: 10.5281/zenodo.19377396

[34] Sharma, V. S. (2026). The Lyman-Alpha Forest in the Big Flare-Up Theory: Absorption Percolation Threshold and Interpretive Non-Uniqueness of the Gunn-Peterson Opacity Rise. BFUT P11. Zenodo. DOI: 10.5281/zenodo.19383804

[35] Sharma, V. S. (2026). The Integrated Sachs-Wolfe Effect in BFUT: Local Spaticle Field Temperature Variations as an Alternative to Decaying Gravitational Potentials in an Accelerating Universe. BFUT P12. Zenodo. DOI: 10.5281/zenodo.19391470

[36] Sharma, V. S. (2026). Weak Gravitational Lensing and the S8 Tension in BFUT: Why Late-Time Clustering Inference Is Not a Unique Test of Lambda-CDM. BFUT P13. Zenodo. DOI: 10.5281/zenodo.19392597

[37] Zwicky, F. (1933). Die Rotverschiebung von extragalaktischen Nebeln. Helvetica Physica Acta, 6, 110-127.

[38] Clowe, D., et al. (2006). A Direct Empirical Proof of the Existence of Dark Matter. The Astrophysical Journal Letters, 648(2), L109-L113.

[39] Sharma, V. S. (2026). Singularity: Why and How Physical Substrate Dynamics Make Infinite Density Impossible. BFUT P26. Zenodo. DOI: 10.5281/zenodo.20557070

[40] Sharma, V. S. (2026). Unification of Particle Physics: Deriving Fine Structure and Coupling Constants, W, Z, and Higgs Boson Masses, Redefining and Unifying Gravity and Time. BFUT P19. Zenodo. DOI: 10.5281/zenodo.20145567

[41] Sharma, V. S. (2026). Light, Photons, and the Universal Speed Limit: A First-Principles Derivation of c from Substrate Condensation Dynamics. BFUT P23. Zenodo. DOI: 10.5281/zenodo.20577935

[42] Sharma, V. S. (2026). The Planck Constant: A First-Principles Derivation of ħ and How It Reshapes the Interpretation of Quantum Mechanics. BFUT P27. Zenodo. DOI: 10.5281/zenodo.20620283

[43] Sharma, V. S. (2026). Black Holes Demystified: What They Actually Are, the Universal Centrality Rule, Why Singularities Cannot Form, and Why Hawking Radiation Doesn't Exist. BFUT P28. Zenodo. DOI: 10.5281/zenodo.20740461

[44] Markevitch, M., Gonzalez, A. H., David, L., Vikhlinin, A., Murray, S., Forman, W., Jones, C., and Tucker, W. (2002). A Textbook Example of a Bow Shock in the Merging Galaxy Cluster 1E 0657-56. The Astrophysical Journal, 567(1), L27-L31.

[45] van Dokkum, P., et al. (2018). A galaxy lacking dark matter. Nature, 555, 629-632.

[46] Menanteau, F., et al. (2012). The Atacama Cosmology Telescope: ACT-CL J0102-4915 “El Gordo,” a Massive Merging Cluster at Redshift 0.87. The Astrophysical Journal, 748(1), 7.

[47] Neeleman, M., Prochaska, J. X., Kanekar, N., and Rafelski, M. (2020). A cold, massive, rotating disk galaxy 1.5 billion years after the Big Bang. Nature, 581, 269-272.

[48] Buzzo, M. L., et al. (2025). A new class of dark matter-free dwarf galaxies? I. Clues from FCC 224, NGC 1052-DF2, and NGC 1052-DF4. Astronomy & Astrophysics, DOI: 10.1051/0004-6361/202453522

[49] Comerón, S., Trujillo, I., Cappellari, M., Buitrago, F., Garduno, L. E., Zaragoza-Cardiel, J., Zinchenko, I. A., Lara-López, M. A., Ferré-Mateu, A., and Dib, S. (2023). The massive relic galaxy NGC 1277 is dark matter deficient. Astronomy & Astrophysics, 677, A104.

[50] Rowland, L. E., Hodge, J., Bouwens, R., Pereira-Santaella, M., Algera, H., et al. (2024). REBELS-25: Discovery of a dynamically cold disc galaxy at z = 7.31. Monthly Notices of the Royal Astronomical Society, 535(3), 2068-2091.